 doi:10.20944/preprints202101.0388.v1

Review

Modelling the dynamics of T-cell development in the thymus

Philippe A. Robert[1]*, Heike Kunze-Schumacher[2], Victor Greiff [1] and Andreas Krueger [2]*

[1] Department of Immunology, University of Oslo, Oslo, Norway
[2] Institute for Molecular Medicine, Goethe University, Frankfurt, Germany

* Correspondence: philippe.robert@ens-lyon.org; andreas.krueger@kgu.de

Abstract: The thymus hosts the development of a specific type of adaptive immune cells called T cells. T cells orchestrate the adaptive immune response through recognition of antigen by the highly variable T-cell receptor (TCR). T-cell development is a tightly coordinated process comprising lineage commitment, somatic recombination of Tcr gene loci and selection for functional, but non-self-reactive TCRs, all interspersed with massive proliferation and cell death. Thus, the thymus produces a pool of T cells throughout life capable of responding to virtually any exogenous attack while preserving the body through self-tolerance. The thymus has been of considerable interest to both immunologists and theoretical biologists due to its multiscale quantitative properties, bridging molecular binding, population dynamics and polyclonal repertoire specificity. Here, we review mathematical modelling strategies that were reported to help understand the flexible dynamics of the highly dividing and dying thymic cell populations. Furthermore, we summarize the current challenges to estimating *in vivo* cellular dynamics and to reaching a next-generation multiscale picture of T-cell development.

Keywords: Thymic selection; T-cell development; T-cell receptor (TCR); mathematical modelling; multiscale models; complex systems; ordinary differential equations (ODE); agent-based models.

Citation: Robert, PA.; Kunze-Schumacher, H.; Greiff, V.; Krueger, A. Modelling the dynamics of T-cell development in the thymus. *Entropy* **2021**, *1*, 0. https://dx.doi.org/10.3390/e10100 00

1. Introduction

The thymus is a unique environment. It is the site of T-cell development. At steady state, it is dependent on continual colonization by a very low number of bone-marrow derived progenitor cells (for review see [1]). In the absence of an influx of T-lineage competent progenitors, T-cell development may be sustained for extended periods of time [2,3]. Thymic size and output are dynamic. The thymus gradually involutes with age, and can transiently shrink up to 90% under stress, pregnancy or infection [4]. Surface markers allowed delineation of many subpopulations of developing T cells (the thymocytes), corresponding to key steps of development and selection. Their dynamics have been extensively measured *in vivo* following organ reconstitution after irradiation, injection of labelled progenitors, thymic grafts, or *in vivo* labelling. Further, the development of thymocytes involves the decision to differentiate into several downstream populations either carrying an $\alpha\beta$TCR, as CD8 T cells, Foxp3$^-$ CD4 T cells, Foxp3$^+$ regulatory T cells, but also as unconventional T cells carrying either $\alpha\beta$ or $\gamma\delta$ TCRs [5]. This complexity has sparked the design of population-based mathematical models to understand the dynamical properties of T-cell development and differentiation in the thymus, and predicted the existence of feedback regulation yet to be verified experimentally. Interestingly, despite the large amount of available data, it is still

Preprints (www.preprints.org) | NOT PEER-REVIEWED | Posted: 19 January 2021 doi:10.20944/preprints202101.0388.v1

very tedious to identify the death and proliferative behavior of thymocytes, in particular the duration of their cell cycle. This knowledge gap limits our understanding of the quantitative regulation controlling T-cell development, and mathematical models are well suited to infer such quantitative parameters hidden inside complex experimental datasets.

The thymus is also known for its substantial quality control of thymocytes. After they have somatically rearranged their TCR loci by V(D)J recombination, it has been estimated that more than 90% of thymocytes die through a process called thymic selection (see section 4). At the molecular level, a prototypical $\alpha\beta$TCR binds to a complex composed of major histocompatibility complex proteins (MHC type I or II) and a small peptide antigen (pMHC). MHC complexes allow cells from the body to present the peptidic signatures of their intracellular content to the T cells. At the cellular level, a thymocyte sequentially interacts with many cells, including dendritic cells, cortical thymic epithelial cells and medullary thymic epithelial cells that present a large sampling of all proteins of our body, the self-antigens, as a training initiation. Thymocytes with non-productive TCR gene rearrangements or expressing TCRs with low affinity to MHC proteins do not survive and undergo "death by neglect". Successful formation of a TCR capable of recognizing pMHC results in positive selection. Developing T cells whose TCR has high affinity for self-peptides are eliminated in a process termed negative selection. It is only partially understood how TCR signaling received through sequential interactions with MHC-self-peptides is integrated into apoptosis or differentiation. However, there is evidence that both kinetic and spatial differences in activation of signaling modules downstream of the TCR contribute to discriminating positively and negatively selecting pMHC ligands [6–10] and it has been proposed that these differences integrate the duration of pMHC-TCR interactions [11]. It remains unknown how single cell decisions explain the population dynamics of the thymus.

Here, we complement previous reviews on thymic selection theories [12] and quantification of T-cell development [13] by providing an updated view of mathematical modelling approaches of the dynamics of T-cell development in the thymus. We deliberately omit mathematical models studying the quantitative impact of positive and negative selection onto the produced repertoire, pathogen escape or MHC recognition, which are already comprehensively described in [12] and were not extensively revisited since then. Instead, we focus on the complexity of inferring *in vivo* T-cell development properties from sometimes indirect experimental settings. Every model relies on assumptions and simplifications needed to match the complexity of the available experimental dataset. We discuss how experimental and model design limitations may be overcome in future studies.

After describing population dynamic models, models to infer cell cycle speed in the thymus *in vivo*, and estimation of cell death through the selection steps, we highlight pioneering models that link thymocyte motility and signaling cell fate and dynamics. We discuss how next-generation models may be formulated in the context of novel high-throughput TCR sequencing technologies.

2. A journey through population models of T-cell development

The main steps of T-cell development in the thymus are depicted in Figure 1A and described in Box 1. The earliest T-cell progenitors in the thymus form a subset of the so-called DN1 (double negative, lacking the expression of CD4 and CD8) cells and are also referred to as Early T-lineage Progenitors (ETP) [14,15]. They arise from bone marrow derived cells transiting via the blood. It has been estimated that only a few cells can enter the murine thymus, with a model of 'gated entry' where one cell can fill one out of 160 available niches [16,17]. The mechanisms underlying gated entry

Preprints (www.preprints.org) | NOT PEER-REVIEWED | Posted: 19 January 2021 doi:10.20944/preprints202101.0388.v1

remain elusive. Periodic alterations in levels of chemoattractants as well as, yet to be molecularly defined, gated release of progenitors from the bone marrow have been proposed [18,19]. Once inside the thymus, an ETP undergoes multiple divisions before sequentially becoming DN2, DN3 and DN4 based on expression of the surface markers CD25 and CD44 [20,21] (Figure 1B).

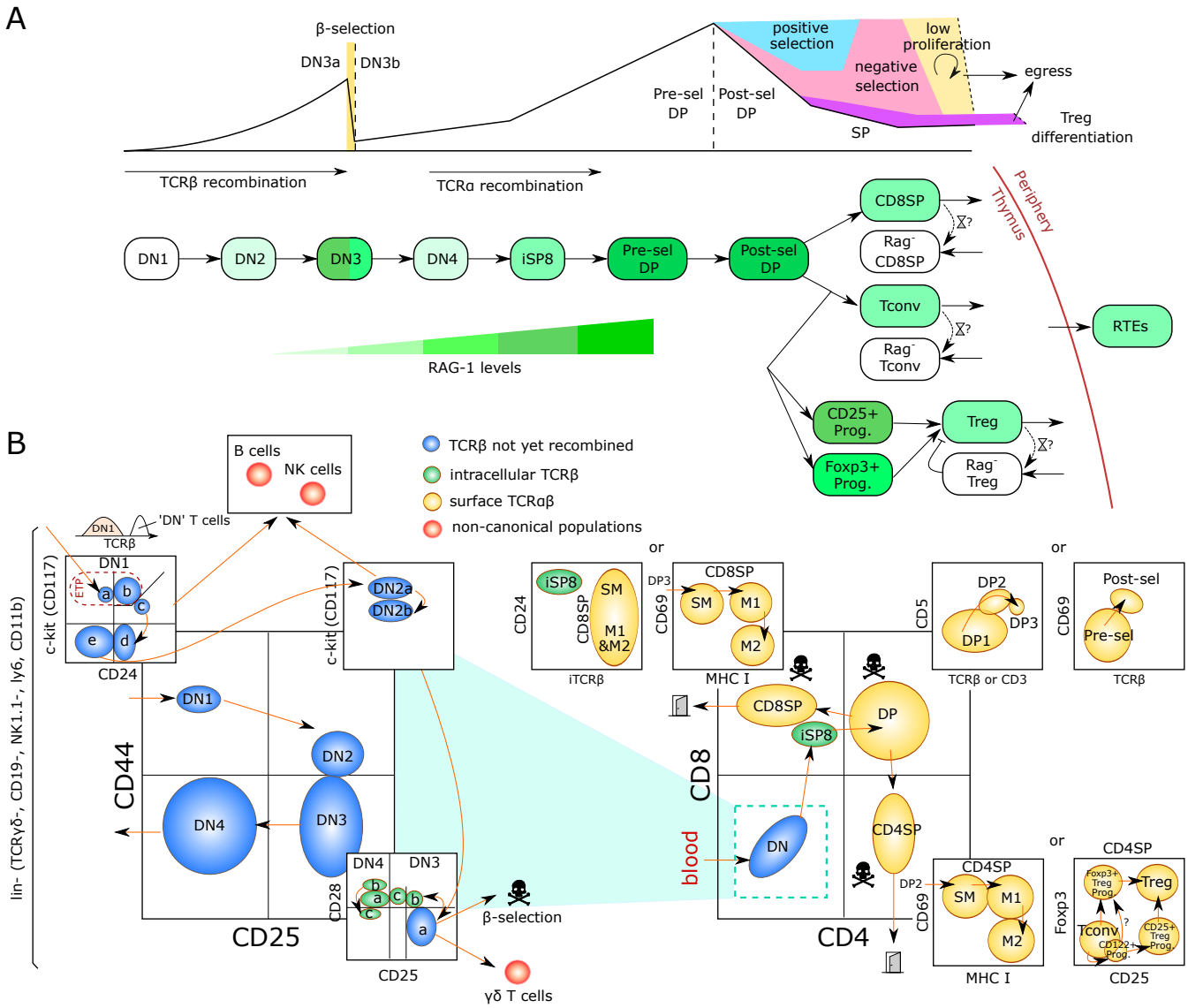

Figure 1. Major developmental steps in the thymus as a basis for population models of T-cell development. (**a**) Main stages annotated with their degree of expansion and RAG1 expression (green levels). RAG1 levels can be used as a timer and distinguish newly generated versus recirculating or long-term populations. The main bottlenecks in transition between thymocyte populations are β-selection, selecting for cells with functionally recombined TCRβ, and positive and negative selection that select for cells with functional MHC reactive, but not self-reactive fully expressed TCR$\alpha\beta$. (**b**) Gating strategies of functional sub-populations. The first lineage gating 'lin-' on the left discards B, NK and myeloid cells. When the DN4 population is only gated on $CD4^{-}CD8^{-}CD28^{-}CD44^{-}$, it also contains more differentiated populations containing TCRβ [22]. DN1 and early DN2a cells can also differentiate into B or NK cells while only late DN2bs are fully committed to the T-cell lineage [23]. The relative size of each compartment is detailed in [22].

Preprints (www.preprints.org) | NOT PEER-REVIEWED | Posted: 19 January 2021 doi:10.20944/preprints202101.0388.v1

Box 1 : Trajectory of murine intrathymic T-cell development.

Thymocytes can be broadly characterized based on their surface expression of the co-receptors CD4 and CD8. The most immature thymocytes are negative for both co-receptors and are hence referred to as double-negative (DN). They give rise to CD4 and CD8 double-positive (DP) thymocytes followed by loss of one of the co-receptors to form CD4 or CD8 single-positive (SP) mature thymocytes, which egress from the thymus after final maturation. Upon entry into the thymus, bone-marrow derived progenitors give rise to early T lineage progenitors (ETPs), phenotypically characterized as $CD44^{hi}CD117^{hi}CD25^{-}$. ETPs constitute a subpopulation of the heterogeneous DN1 ($CD44^{hi}CD25^{-}$) population. Acquisition of CD25 marks the next developmental DN2 stage. At this stage, T lineage commitment is completed and pre-commitment and post-commitment DN2 thymocytes are referred to as DN2a and DN2b, respectively. DN2b cells express somewhat lower levels of CD117, which progressively decline towards the $CD44^{-}CD25^{+}$ DN3 stage. V(D)J recombination of Tcrb, Tcrg and Tcrd loci commences at the DN2b stage and continues in a subset of small DN3 cells, termed DN3a ($CD44^{-}CD25^{hi}CD27^{-}CD28^{-}$). Upon successful V(D)J recombination, DN3a cells give rise to either $\gamma\delta$T cells or large DN3b cells ($CD44^{-}CD25^{int}CD27^{+}CD28^{+}$) in a process called β-selection. Progressive loss of CD25 marks the DN4 compartment, which in turn gives rise to pre-selection DP thymocytes ($CD4^{+}CD8^{+}TCR\alpha\beta^{low/neg}CD69^{-}CD5^{-}$) via an immature $CD4^{-}CD8^{+}TCR\alpha\beta^{-}$ (ISP) intermediate. At the pre-selection DP stage rearrangement of the Tcra locus occurs followed by the initiation of selection. Positively selected DP thymocytes up-regulate the $\alpha\beta$TCR and acquire expression of CD69 and CD5. Loss of one co-receptor marks generation of CD4 and CD8 SP thymocytes, whose maturation is further characterized by loss of CD69 and CD24 as well as acquisition of CD62L and MHC-I.

2.1. Early steps of thymus development

The dynamics of DN1 to DN4 cells have been monitored by injection of congenic bone-marrow derived progenitors [24]. Injected cells remained at the DN1 stage for 10–12 days while transition through the DN2 population was short as DN3 cells appeared after as early as 11 days, and DN4 cells after day 14–15. A mathematical model from Manesso and colleagues [25] used this dataset to compare different proliferation model structures for the DN1 population. The types of equations are depicted in Figure 2A and the model structure in Figure 2B. The best model fit predicts that cells would remain in DN1 for up to 11 divisions before transitioning to DN2s, spending on average 1 day per cycle. Interestingly, no other hypotheses, in which cells would leave the DN1 stage after fewer divisions, or with more distributed probabilities to leave DN1 at earlier divisions, could explain the data well, revealing a synchronization of the cells to leave after a certain number of divisions (or time). This prediction was further experimentally supported by showing a higher differentiation potential of late DN1s [25] as well as progressive transcriptional changes allowing the definition of a developmental trajectory within ETPs [26].

Although identified parameters for the DN1 population and the synchronization statement were robust to the Porritt dataset [24], the inferred residence or cycling times for the DN3 and DN4 populations were not identifiable from this dataset, meaning the exact same curves can be reproduced with different cycling speed of these populations due to compensation between parameters. This means additional experimental constraints would be required to also fix the DN3 and DN4 dynamical parameters, and likely comes from the fact that the dataset could only monitor the frequencies of labelled donor cells rather than absolute numbers, possibly due to a high variation of progenitor engraftment among transplanted mice. Altogether, the model was useful to uncover the synchronized behavior of DN1s and suggest 11 divisions in 11 days for these particular cells. Notably, the study by Porritt and colleagues employed a purification strategy of donor cells that omitted some progenitor subsets with the potential of thymus colonization and more rapid intrathymic differentiation kinetics [27,28].

Preprints (www.preprints.org) | NOT PEER-REVIEWED | Posted: 19 January 2021 doi:10.20944/preprints202101.0388.v1

Since every 9 to 12 days a new wave of progenitors is initiated [17], it raises the question how thymus size is maintained over time, and in particular, whether cyclic colonization by progenitors would induce detectable fluctuations. The 'synchronous development hypothesis' states that the periodic seeding induces such fluctuations, while an opposing hypothesis argues that an asynchronous release of seeders or the existence of size regulation within DN populations could smoothen such fluctuations to undetectable levels. Cai et al [29] developed a model of DN2-3, DN4 and the subsequent DP compartment without any size regulation and predicted fluctuations to be around 40% amplitude for the DP and total thymocyte populations while DN4 and SP would be quite stable. If this were true, this would mean to expect a high biological variation between different unsynchronized mice. The authors propose a statistical test based on plotting different populations in the same x-y axis, expected to show an ellipse from only one experimental time-point, if such fluctuations exist. The prediction has not yet been verified. As a replacement for a direct longitudinal analysis of thymocyte numbers, that is not possible, an approximation via ultrasound-based determination of thymus size might be an alternative valid approach.

Bone-marrow derived thymus seeding progenitors most likely comprise multiple cell types, including IL-7R$^+$ CLPs (common lymphoid progenitor), Flt3$^+$ LMPPs (lymphoid-primed multipotent progenitors) and possibly others, as well as phenotypically ill-defined intermediates [1,27,28,30,31]. For instance, *in vivo*, CLPs displayed a more rapid differentiation into DP thymocytes when compared to LMPPs, suggesting that population heterogeneity of thymus seeding progenitors could contribute to continuous thymic output despite gated entry [13,28].

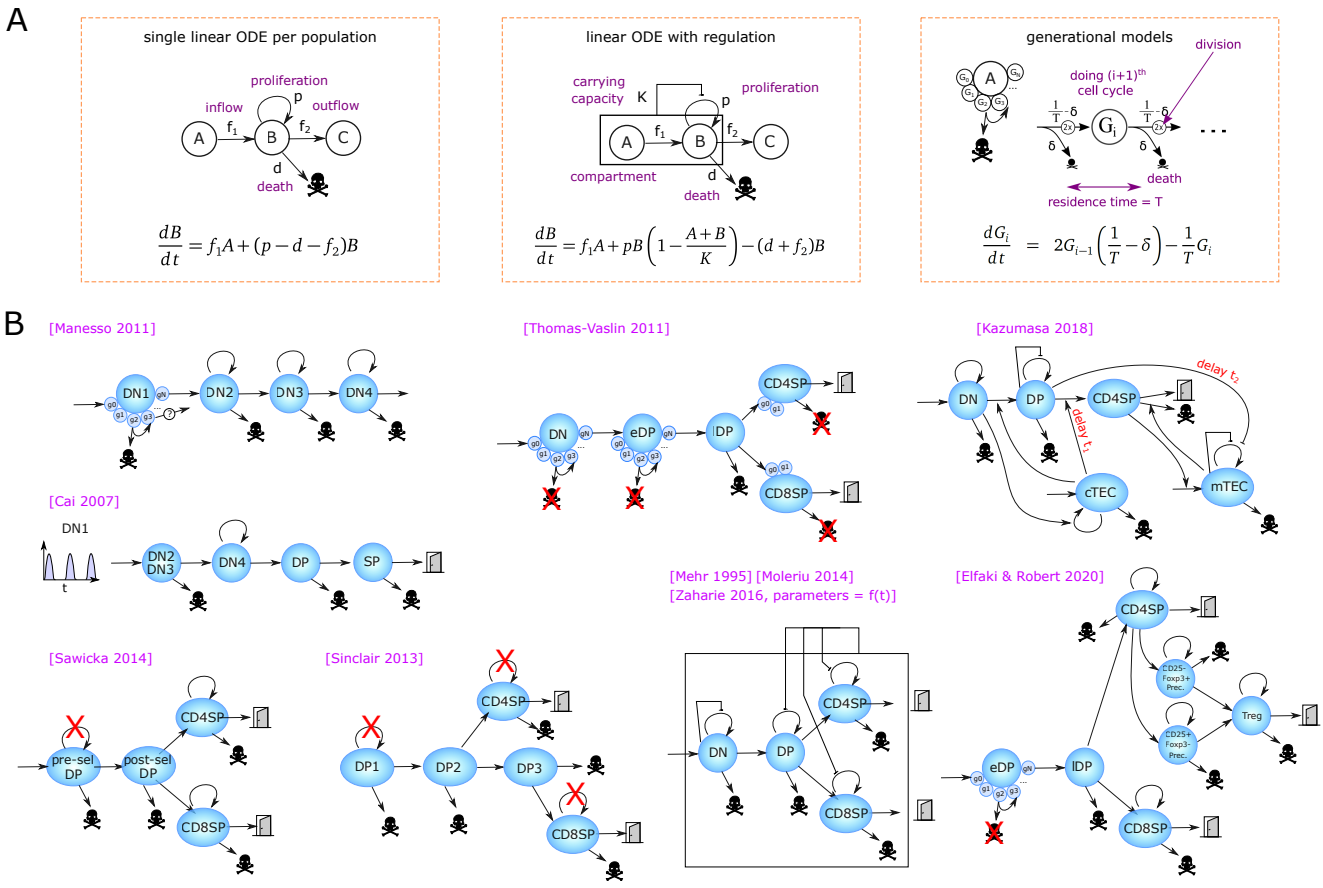

Figure 2. Population dynamics mathematical models of the thymus. (**a**) Types of equations used when simulating thymic population dynamics: simple ODE with proliferation, death and differentiation (left), with an additional regulated logistic growth according to a maximum carrying capacity K (middle) or generational models that simulate the cell numbers at each division within a compartment (right). (**b**) Published mathematical models, following the equation design explained in A. The red crosses denote neglected mechanisms in the models.

Preprints (www.preprints.org) | NOT PEER-REVIEWED | Posted: 19 January 2021 doi:10.20944/preprints202101.0388.v1

In general, despite possible variations due to the periodic seeding over weeks and the slow thymic involution over years, most models for thymic populations could fairly consider every population to be at 'steady state' during the time of simulation (a few days typically). During the next steps of DN development, the Tcrb locus is genetically recombined and in-frame recombination results first in expression of TCRβ in complex with a surrogate pre-TCRα chain, defining completion of the DN3a stage [32]. Somatic recombination is accompanied by cessation of proliferation and death of cells that fail to productively recombine the Tcrb locus, called β-selection (Figure 1A,B), estimated to kill around 70% of the cells through this checkpoint [33]. Productive recombination of TCR$\gamma\delta$ can also happen at this stage and lead to the separate differentiation of $\gamma\delta$T cells (Figure 1B). The DN3b and DN4 stages are highly proliferative, and are accompanied by upregulation of CD8, then both CD4 and CD8 to become 'immature SP8' (iSP8) then 'Double Positive' thymocytes (DP), respectively. The latter can be further separated as 'pre-selection' DPs and 'post-selection DPs' (Figure 1B). Maturation from DN3b to pre-selection DP is a continuous process that comprises massive proliferation followed by recombination of the Tcra locus. Selection is then initiated to probe for formation of a functional TCR$\alpha\beta$ complex expressed on the surface. Failure results in death by neglect, which also eliminates cells with $\alpha\beta$TCRs with low affinity interactions for pMHC. Successful positive selection is accompanied by expression of activation markers like CD69. DPs with surface expression of a functional $\alpha\beta$TCR are also the first population to be probed for high-affinity pMHC interactions during negative selection resulting in massive cell death [34] (see section). The final step of T-cell development is the choice between becoming a $CD4^{-}CD8^{+}$ single positive T cell (future CD8 cytotoxic T cell) or a $CD4^{+}CD8^{-}$ single positive T cell, (future conventional CD4 T helper cell (Tconv) or $Foxp3^{+}$ (Treg cell). With the exception of Treg-cell precursors, the SP populations are not particularly proliferating, although the mature 2 (M2) stages of CD4SP and CD8SP (Figure 2B) are able to proliferate upon stimulation [35]. Indeed, analysis of mice expressing an H2B-GFP reporter in the TCRδ locus substantiated the hypothesis that thymocytes post selection and during maturation undergo one or two rounds of division [36]. Further, using TCR-transgenic mice, Le Campion et al. showed that proliferation strength in the SP stage *in vivo* is related to the MHC settings and quantitatively impacts on the thymic output [37], showing that clonal lineages might selectively be expanded at this late stage.

Apart from the studies from Manesso et al. [25], Cai et al. [29], analysis of the DN differentiation steps by mathematical modelling has been scarce. A recent transcriptional multiscale model by Olariu et al. [38] is discussed in Section 5. Most other thymic models considered the combined DN stages as one compartment (mainly because DN datasets were poor at the time). The original naming of populations into DN1 to DN4 is biologically inconvenient because DN3a cells are more similar to DN2 than DN3b, which in turn are similar to DN4 forming a continuum that is likely to extend to DP cells prior to initiation of Tcra rearrangement. Therefore, one would need to be careful which compartments to simulate and how to associate death and proliferation at the proper stage. The DN2-3a and DN3b-DN4 could possibly be merged as functional compartments, and one would expect a high death rate at the DN3a - DN3b transition.

The next level of models simulate the major populations of the full thymus, selected according to the biological question of interest.

2.2. Estimation of the flow between compartments at steady state using larger models

Inferring the duration of each developmental stage and the flow of cells between them at steady state has been approached both experimentally and mathematically.

Preprints (www.preprints.org) | NOT PEER-REVIEWED | Posted: 19 January 2021 doi:10.20944/preprints202101.0388.v1

Turnover of thymocyte populations has been estimated based on *in vivo* labelling of cells with nucleoside analogues, such as [3H]-thymidine, BrdU and EdU. These labels are incorporated into the cell's DNA during replication, i.e. they label actively cycling cells. Label incorporation is detected through autoradiography, antibodies, and click chemistry, respectively. Administration of a single pulse allows determination of the frequency of actively cycling cells (see section 3), whereas continuous labelling allows to determine turnover within a population by measuring replacement of non-labeled with labeled cells or vice versa. Continuous labelling cannot discriminate between intra-population proliferation and influx of labeled progenitors. Similarly, discrimination between death and outflux of non-labeled progenitors is impossible. Thus, both pulsed and continuous labelling have to be complemented with additional assays or mathematical inference to discriminate between these parameters.

Using such sets of experiments, the life-time of DP thymocytes has been determined to be 3.5 days [39]. Given that most DP cells have a comparatively low rate of proliferation, whereas all DN4 precursors proliferate rapidly, the majority of label accumulation can be ascribed to influx. The same study indicated a fraction of only 3% of DP cells becoming SP based on the flow of label to the next generation. A gap in the acquisition of label in SP cells supported the notion that they were largely non-cycling, and their life-time was estimated to be 12 to 14 days, which may be an overestimate, potentially due to the presence of thymus-resident cells. Analysis of cellular flow through more immature populations was complicated by proliferating populations being interspersed with less proliferating ones [33,40]. These limitations were partially overcome by the use of RAG-deficient and TCR-transgenic strains to interfere with developmental checkpoints [33]. Together these studies revealed population heterogeneity of the DN3 population, consistent with the later identification of DN3a and DN3b subsets [40]. Together, it was proposed that thymocytes undergo approximately 10 divisions between the DN3 to the DP population, and that 70% of DN3 thymocytes die at the β-selection checkpoint [33].

A more recent continuous labelling study showed that most pre-selection DP became post-selection DP within 4 to 5 days (although they might still proliferate and would never reach 100%) [41], and that they display massive caspase activation after 3 days. Using continuous labelling as well, [42] showed that post-selection DPs become fully labelled in 3 to 4 days; naive CD8SP and CD4SP gradually become labeled between day 2 and 8. This shows that the post-selection DP stage is around 3 to 4 days, while the replenishment of CD4 and CD8 might not be synchronous, some cells becoming single positive more rapidly than others, thus refining the earlier study by Egerton and colleagues [39]. Sinclair et al. [43,44] used a tetracycline inducible Tet murine model, where TCR signaling is blocked by default and developing thymocytes are stuck at the pre-selection DP stage. Treatment with tetracycline rescues T-cell signaling, leading to a synchronized wave of cells from the pre-selection DP stage through positive and negative selections.

In parallel, several mathematical models have been developed in order to estimate how many cells transit between the populations (Figure 2B). A founding model was published in 1995 [45] for DN, DP, CD4SP and CD8SP populations, where the DN compartment is regulated by logistic growth, and DP and SP populations being regulated by the size of the full thymus. Although no kinetic datasets were available at the time, realistic boundaries for the model parameters were inferred from steady state, from qualitative knowledge and developmental timing known at the time.

As a follow-up, Sawicka et al. [46] have used steady state values from WT mice to identify the flow of cells entering and leaving the DP and SP compartments with single ODEs per population but without size regulation since it is based on steady-state. They assumed that SP proliferate but not DP thymocytes. Including newer estimations of death by selection from [34], they identified that 35 million cells would enter the DP

Preprints (www.preprints.org) | NOT PEER-REVIEWED | Posted: 19 January 2021 doi:10.20944/preprints202101.0388.v1

compartment per day, and give realistic death rates, proliferation and export in each compartment to match the previously estimated residence times in the thymus. The lack of proliferation in the pre-selection DP compartment likely over-estimates the inflow of cells in the DP compartment, which is probably in the order of a few millions per day since the upstream DN3-DN4 compartment is typically less than 4 million cells (depending on the murine background and age).

A major step for evaluating cell flow rates was the experimental measurement of a developmental wave through the DP and SP populations. The model of Sinclair et al. [43,44] has used the tetracycline-induced developmental wave of cells through post-selection DP and SP stages to infer the flow of cells through CD4 and CD8 differentiation and selection. Their model consists of linear ODEs (Figure 2B), and delineates a 2-step differentiation pathway for CD4 (DP1 and DP2) and a 3-steps pathway for CD8 T cells (DP1 to DP3), which are believed to differentiate later from DP thymocytes. T cells with CD8 or CD4 biased TCRs evolve as separate populations with different parameters, and DP1 refers to pre-selection DP. The authors did not assume proliferation at any stage, restricting the main factors to be death, forward differentiation and thymic output. The ratio between death and output at the last stage was inferred by an additional experimental blockade of trafficking using FTY720 treatment [47]. The authors confirmed the robustness of the inferred parameters by bootstrapping, and estimated 6.3 and 9.5 days respectively between entry into DP and exit as fully mature CD4 and CD8 T cells. In the model, the larger steady state amount of CD4 SP cells in the thymus compared to CD8 SP cells was not due to a preferential differentiation into CD4 (nor an imbalance in TCR-bias among pre-selection cells), but rather a much larger death rate of CD8-biased T cells during DP stages. The authors discussed a limitation of the inducible Tet experimental system, where T cells show a skewed CD4 vs. CD8 differentiation ratio in comparison to WT mice, likely due to the manipulation of TCR signaling. Although the hypothesis of non-proliferation in post-selection DP stages is experimentally supported, exclusion of limited proliferation in SP [36] and pre-selection DP cells might slightly affect the identified parameters, yet including proliferation would likely create structural correlation between parameters and require additional experimental data to separate proliferation rates from death/export.

2.3. Models for thymus involution and shrinkage

A second line of models have used dynamic perturbations to infer dynamical properties of T-cell development in the thymus. Some of them have been used to compare mechanistic hypotheses to explain the perturbation.

The thymus shows an intriguingly dynamic cellularity during life. First, its size progressively involutes with time, associated with a decrease in both proliferation and survival of the cells [48]. Second, it considerably shrinks following pathophysiological perturbations like infection, stress, chemotherapy or malnutrition [4]. For instance, Trypanosoma cruzi infection induces a slow decay of all populations during 15-20 days and is associated with DP thymocyte death and the unexpected presence of DP cells in the periphery [49]. Pregnancy also induces thymic atrophy on a longer period [50], which could be induced by injection of oestradiol in non-pregnant mice. Oestradiol-induced atrophy was linked with loss of DN cells and reduced proliferation after β-selection, but did not seem to affect DP cells although Treg-cell development was altered [51]. Thymic atrophy in the context of acute or viral infection like influenza has gained interest due to recent reports showing the presence of the virus in the thymus [52], either by direct infection due to proximity with the lungs, or imported by migratory APCs coming from the lung [53], which might present foreign antigens as self during selection.

Preprints (www.preprints.org) | NOT PEER-REVIEWED | Posted: 19 January 2021 doi:10.20944/preprints202101.0388.v1

A first full thymus model built on experimental kinetics has been introduced by Thomas-Vaslin et al. [54]. The authors induced death of proliferating cells and measured the dynamics of thymus shrinkage and recovery, using a conditional suicide gene and injection of an activating compound. The data helped to calibrate a model where DN, early DP (pre-selection DPs) and SP cells can proliferate, while late DPs die by (positive or negative) selection. Interestingly, instead of a single linear ODE per population, they developed a generational model for each proliferating compartment (Figure 2A,B) with a fixed number of divisions (with a fraction of cells exiting before the last division to have smooth average numbers of divisions). From an estimation of 20,000 cells per day entering the DN compartment, they assume that DN cells divide 4 times, during a period of 18 days, while early DPs proliferate 5 to 6 times with high speed (4 to 5 divisions per day). Explaining the experimental rebound requested a very high speed of early DP division in the model. They also estimate that CD4SP and CD8SP would divide between 1 and 2 times and provide an estimation of thymic flow of cells between each compartment including the spleen and lymph nodes together with estimated residence times in each compartment that was consistent with literature.

Newer findings would suggest possible adaptations in the model design. The inflow of 20,000 cells per day entering the DN suggests the DN compartment was referring to DN2-DN3-DN4, as DN1 cells harbor many divisions [25]. The slow proliferation of DN cells with 4.5 divisions in 18 days could be compensated by including death by β-selection, in which case the cells would divide more and faster. Further, separation of the DN compartment into pre- and post-β-selection DNs could allow for higher proliferation of the DN3b-DN4 compartment. In turn, this could result in an increased flow of cells entering the early DP population, therefore requiring more realistic, slower divisions at the early DP stage to get the fast rebound. Finally, the absence of simultaneous proliferation and death, estimated as a single parameter, could be re-interpreted with newer experimental estimates of cell death.

Altogether, the model of Thomas-Vaslin et al. [54] brought substantial contributions to the field. First, it showed that it is possible to explain the dynamics of this strong experimental perturbation with a simple model and without any size regulation nor feedback. Indeed, we have noticed that single linear ODE models typically need to include a logistic growth to get a faster recovery. It is likely that the generational model of Thomas-Vaslin allows for faster reconstitution because cells cannot progress to the next developmental stage until a few divisions whereas linear ODE models have a constant exit rate. Second, the separation of proliferating early DP and highly dying late DP compartments has a realistic model structure and replicated the time-resolved experimental perturbation dataset, suggesting it can be re-used to build more precise models with newer hypotheses like the one provided by Elfaki et al. [55]. Third, their experimental dataset is valuable to test any new model for T-cell development.

As a different source of atrophy, Moleriu et al. induced thymic atrophy by dexamethasone injection in mice, which triggers cell death, as a surrogate to mimic stress-induced atrophy [56], and used Mehr's model to identify population dynamical parameters [45]. The dynamics of dexamethasone in the blood are modelled as different possible time-dependent functions. The effect of dexamethasone is modelled as perturbation at the level of proliferation, death, or transfer rates, proportional to the dexamethasone levels. The same dynamics of perturbation applied to all DP and SP populations was not successful in replicating the dynamics, but rather each population needed a perturbation with different strength/dynamics. They also showed that in the model, the proliferation rate and the carrying capacity of the populations were structurally correlated (they compensate each-other), meaning that one parameter needs to be fixed arbitrarily, or maybe that a regulation of population sizes is not necessary to explain this dataset. It is unclear whether the atrophy could be explained by a simpler perturbation model using a different differentiation model structure. For instance, in Elfaki et al. [55], atrophy

Preprints (www.preprints.org) | NOT PEER-REVIEWED | Posted: 19 January 2021 doi:10.20944/preprints202101.0388.v1

could already be well explained by the dynamic perturbation of only one compartment (increasing death of DP cells). Altogether, Moleriu et al. have provided a detailed explanation how far Mehr's model can be used to infer dynamics of thymic populations.

Recirculating SP thymocytes have meanwhile been identified based on RAG expression, and previous models did not include the development of Treg cells. To this end, Elfaki et al. followed influenza-induced thymic atrophy in mice [55], reaching a 90% shrinkage in cellularity 7 to 10 days after infection, followed by a very fast recovery of 3-4 days, without prior knowledge on the mechanisms of atrophy. The authors used a RAG1^{GFP} reporter to distinguish newly-generated, RAG$^+$ cells from resident or recirculating cells and asked whether influenza would skew the differentiation of T-cell populations, including Treg cells. By following the dynamics of the main populations during influenza-induced atrophy, they could show that only RAG$^+$ newly generated cells were impacted. The diversity of the Treg TCR repertoire was lower at the peak of atrophy, and the frequencies of Treg populations appeared to be transiently increased. In order to disentangle the mechanisms by which influenza induces atrophy, they developed a mathematical model, based on the early DP - late DP compartments of Thomas-Vaslin [54]. They adapted the SP populations to include three different generation pathways for Treg cells, using single ODEs with proliferation and death, and fixing most parameters from literature (Figure 2B). Most parameters for Treg generation are unknown and were fitted. Death, proliferation and output of each SP population were structurally correlated, so the authors could fix their sum (death + output – proliferation) from steady state constraints and experimental residence times. The dynamics of atrophy were completely insensitive to the contribution of death versus output and proliferation provided their sum was constant. The mechanistic impact of influenza did not seem to be direct, as influenza viremia peaks typically much earlier than the peak of atrophy at day 10, suggesting the existence of a downstream factor inducing atrophy, such as glucocorticoids or IFN-γ production by NK or CD8$\alpha\alpha$ cells [55]. Therefore, the authors hypothesized a downstream factor of unknown timing, as a Gaussian perturbation to select population death or differentiation. Interestingly, transiently increased DP death alone could explain well the dynamics of all DP and SP populations, including the observed transient increase of Treg cells as a fraction of the CD4SP compartment. This peak was a dynamical artifact likely due to different life-times, where Tconvs decay faster than Foxp3$^+$ populations and the frequency of the latter transiently increases as an overshoot. Modulation of Treg differentiation did not help to explain the data better, but instead, an increased export of all SP thymocytes could improve the fit. This shows the importance of mathematical modelling in understanding the dynamic behavior of populations under perturbations. Consistent with previously defined differentiation trajectories of Tregs [57,58], generation of Treg precursors from CD4SP cells rather than directly from DP precursors provided the best explanation of the data in the study of Elfaki et al. [55], showing that the dynamical perturbation included biological information on Treg ontogeny. It remains an open question, how thymic atrophy decreases Treg TCR diversity and whether this leaves an imprint on the generated repertoire through life. The model showed that the total increased export is minor, meaning that a difference in exported TCR diversity might not have a strong effect on the peripheral repertoire. An agent-based model with cells carrying diverse TCRs could help linking population dynamics to TCR diversity and uncover potential regulatory mechanisms. For instance, reduced Treg diversity could arise from a 'wrong' timing of crossing the cortico-medullary junction that is a region with increased antigen presentation. Indeed, modification of thymocyte migration between cortex and medulla does not change the amount of generated Tregs [59,60] but likely impacts the type of encountered antigens. Alternatively, *de novo* Treg formation could occur via different developmental intermediates, which generate Tregs of distinct self-reactivity and functionality [61,62]. Such agent-based model could explain why a change in diversity is unnoticed when it comes to dynamics.

Preprints (www.preprints.org) | NOT PEER-REVIEWED | Posted: 19 January 2021 doi:10.20944/preprints202101.0388.v1

Finally, the natural thymic size involution during the very early stages of development has been modelled in the study by Zaharie et al. using a linear ODE model [63] adapted from Mehr and Moleriu's models (Figure 2B). Pre-natal and post-birth development are simulated with two different sets of parameters, and thymic involution with age is simulated as an exponentially decreasing proliferation rate of each compartment with time. It remains intriguing why the two developmental phases need two sets of parameters and suggest the existence of a common regulatory mechanism to consider for future models.

2.4. Regulations between thymic populations

The above-presented models have supposed a certain level of independence between the different cell fates. This is consistent with the essentially linear developmental trajectory of thymocytes from thymus colonization to egress of mature T cells. However, the size of certain thymocyte populations is likely to be subject to constraints, such as availability of survival factors, including cytokines, or cell-cell contacts including interaction with stromal cells or other antigen-presenting cells. The existence of population control or interactions are difficult to validate experimentally. Nevertheless, IL-7 controls overall thymocyte cellularity [64,65]. Notably, in the absence of IL-7 or its receptor, the relative proportions of major populations are retained. Consistently, Almeida et al. [66] used murine background models carrying different amounts of DP cells and showed that the number of SP cells were always proportional to the DP compartment size, suggesting that the SP niche is not smaller in the presence of more DPs. Conversely, in conditions of severely limited thymus colonization, such as in CCR7/CCR9 double-deficient mice, population sizes recover to bona fide wild-type levels at the DN3 stage and beyond [67,68]. Recently, it was suggested that, at least in a model of cellular competition, thymus cellularity is controlled through feedback regulation, in which DN2 and early DN3 cells sense DP population size and tune cell cycle duration in an IL-7-dependent manner accordingly [69]. There is substantial evidence for regulation of mature Treg numbers by IL-2 or IL-15 availability [70]. Competition between T cells for accessing spatially restricted antigens, types of APCs or cytokines could be an additional mechanism balancing the relative amount of each population, and could bring multiple possible fates for thymocytes carrying the exact same TCR, and has not been investigated by mathematical modelling yet. Interestingly, a recent study [71] showed that RAG$^-$ Tregs, resident or recirculating from the periphery, can inhibit the development of newly generated Tregs. We refer to the overview by Klein et al. for details on the complex mechanisms and models for Treg differentiation [72].

Only in some mathematical models, different populations sharing the same 'niche' regulate their relative size in a TCR- and antigen-independent manner through a logistic growth control (Figure 2B). Further, the amount of cells becoming CD4, CD8, or Tregs are pre-encoded into a differentiation rate instead of a homeostatic control between these populations. The capacity of generational models like the one established by Thomas-Vaslin to reproduce fast recovery, would argue that logistic growth is not required, although this model inferred a supra-physiologically high proliferation rate for DPs. As a rare attempt to model population inhibitions, Kaneko et al. [73] analyzed the kinetics of thymic population dynamics after sub-lethal irradiation that leads to profound but transient atrophy. They compared multiple model structures on how the availability of TEC cells (depleted by irradiation) could regulate other populations (Figure 2B), using iterative fittings [74]. Expectedly, a single ODE could not explain the speed of DP reconstitution and needed a logistic growth mechanism. Further, among the different tested scenarios, the model could best explain the data when DN and cTECs were inhibiting each other's dynamics. The authors attempted to explain the dynamics of mTECs only from the dynamics of the DP and SP populations and needed to include multiple mechanisms including i) self-inhibitions of the mTECs and ii) opposite effect of

Preprints (www.preprints.org) | NOT PEER-REVIEWED | Posted: 19 January 2021 doi:10.20944/preprints202101.0388.v1

SP (positive) and DP (negative) on mTEC reconstitution, and/or iii) impact of DN or cTECs onto DP, CD4 or mTECs. The modelling approach generated 5 possible models explaining well the dynamics of mTECs and the authors selected the most biological consistent with existing literature. This example highlights the complexity of identifying unknown negative regulations between populations from kinetic data. Indeed, the combinatorial number of possible interaction networks is huge, and one could expect that many networks can explain the data equally well. Having many consistent models may help narrow down possible mechanisms and prioritize which ones to measure experimentally. Alternatively, one could use the mathematical model to design a new set of minimal experiments that would be sufficient to discard as many remaining possible explanations (models) as possible, as in [75]. This is very tedious.

In general, the study of regulation mechanisms might require modelling techniques adapted to their scale, and for instance spatial competition could eventually be best captured using agent-based models instead of population dynamics ODE models.

3. Estimation of *in vivo* cell proliferation in the thymus

Understanding the strikingly fast dynamics of thymus reconstitution and population size regulation requires to visualize how fast thymic populations actually proliferate *in vivo* and under perturbations. We have mentioned the work of Manesso et al. [25] and Thomas-Vaslin et al. [54] that estimated the division number from population kinetics. Here we focus on experiments (Figure 3A-D) and mathematical models (Figure 4A-G) aiming at measuring and quantifying the duration of the cell cycle and its phases *in vivo* in the thymus.

3.1. Measuring the number of divisions by dye dilution

A first measurement of proliferation involves a dye like CFSE or CTV that stays in the cell and gets diluted during division. The level of remaining dye in comparison with the original intensity levels thus informs on the number of divisions (Figure 3A). This technique has been rarely used to study thymocyte proliferation *in vivo*, because labelling is performed *in vitro* and thus requires isolation and subsequent transfer into the thymus [76]. Nevertheless, dye dilution approaches have been employed to assess divisions of thymocytes *in vitro*, for instance on a supporting layer of OP9-DL1 cells, or using Reconstituted Thymic Organ Cultures (RTOCs). In particular, Kreslavsky et al. [77] observed that 4 to 5 divisions separated the DN3a/DN3b transition to the entry into the DP compartment *in vitro*, indicating that DN3b, DN4 and iSP8 altogether would contain 4 to 5 divisions. The ETP/DN1 compartment has not directly been checked for number of divisions and Manesso et al. suggested 11 divisions [25]. Finally, Yui et al. [23] observed that ETP, DN2a and DN2b cultured *in vitro* were able to proliferate for 3 to 5 divisions in 3 days depending on the population, but did not check when the cells acquired the next phenotype during these divisions, leaving the possibility of transition to the next population. Meanwhile DN3a and DN2b cells proliferated heterogeneously, whereas ETP and DN2a cells showed a fairly homogeneous proliferation. DN3a cells underwent 2 to 4 divisions before downregulating CD25 and becoming DN4. Hare et al. [35] showed that the most mature stage of SP4 and SP8 cells are able to proliferate for multiple divisions in RTOCs under antigen stimuli. Consistently, an *in vivo* study showed that MHC-dependent antigen recognition induced different strengths of proliferation [37]. It is not completely clear whether *in vitro* conditions accurately reproduce the *in vivo* signals controlling proliferation, death or emigration (for instance, RTOC cells might not exit and continue proliferating). Finally, Föhse et al [36] estimated one to two divisions at most from the post-selection DP stage. In general, the number of divisions

Preprints (www.preprints.org) | NOT PEER-REVIEWED | Posted: 19 January 2021 doi:10.20944/preprints202101.0388.v1

has been limited to a qualitative constraint for building models rather than being used as a quantitative training dataset.

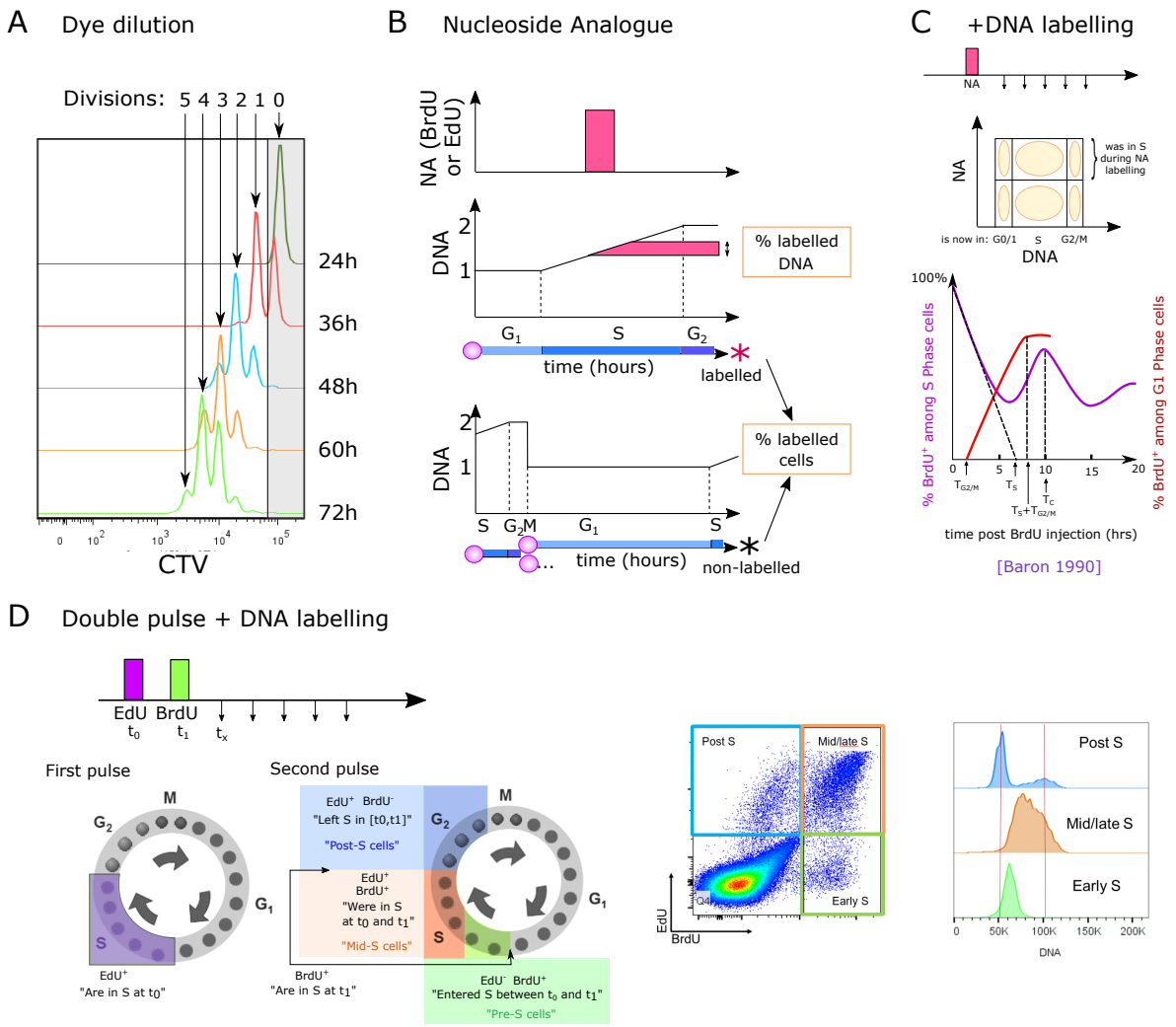

Figure 3. Experimental methods to measure proliferation in the thymus. (**a**) Following the number of divisions of injected labelled cells by dye dilution. (**b**) Following the amount of cells in the S phase by BrdU or EdU injection. (**c**) Tracking of labelled cells at later time-points. (**d**) Dual-pulse labelling with EdU followed by BrdU to label cells that enter or leave the S phase in between pulses and track the cycle stage of the labelled cells later.

Similar to the dilution of labels introduced *in vitro*, dilution of genetic markers may serve as measures for proliferation. Thus, RAG recombinase is stage-specifically expressed in thymocytes undergoing somatic recombination of TCR genes and rapidly shut-off thereafter. Thus, using RAG1-^{GFP} reporter knock-in or transgenic strains, dilution of GFP serves as surrogate for proliferation after termination of TCR gene rearrangement [61,78,79]. To overcome the need for normalization to correct for degradation of GFP encoded by this model, the half-life of GFP has been prolonged to weeks or even months by fusing it to histone 2B [80,81]. Such fusions have been used to generate Tcrd-H2B-GFP mice to label $\gamma\delta$T cells [82]. During recombination of the Tcra locus, Tcrd and thus H2B-GFP coding sequences are excised and protein expression ceases, making H2B-GFP levels virtually exclusively dependent on dilution through proliferation. This system has been used to analyze dynamics of various $\alpha\beta$T-cell populations [36].

Preprints (www.preprints.org) | NOT PEER-REVIEWED | Posted: 19 January 2021 doi:10.20944/preprints202101.0388.v1

3.2. Nucleoside analogue incorporation during S phase

A second approach is to use EdU or BrdU to label actively replicating cells, as described in (Section 2). We deliberately omit older studies using Thymidine labelling because the dye was later found to be re-incorporated by cycling cells from dead cells [83]. It has been estimated that BrdU has a half-life of only 12 min in mice and bioavailability of BrdU is lost 60 min after administration [84,85]. Thus, it is well-suited for short-term pulse labelling of cells.

3.2.1. Direct EdU or BrdU staining

Direct EdU or BrdU staining reveals cells that are currently incorporating DNA It can be used *ex vivo* to label the cells currently in the S phase, or *in vivo* (Figure 3B) to measure the percent of labelled cells (i.e., that were in S phase during the labelling pulse) or the amount of labelled DNA inside these cells, and possibly to track them at later time-points. This technique does not directly indicate proliferation speed nor the frequency of cycling cells, because it does not provide information on the duration of G1, G2 or M phases. For instance, the same BrdU labelling could be generated either by all cells cycling with a long G1 phase, or by only a fraction of cells cycling with a short G1 while the rest would be quiescent. BrdU labelling has widely been used to compare the cycling speed of different populations, but it therefore can be misleading, if the populations have different G1+G2M durations, or if they contain different proportions of quiescent cells. Nevertheless, very low frequencies of labelled cells are an indicator of low proliferation percent or speed (extremely long G1 for instance).

Such methods have revealed that all DN populations are highly proliferating except the DN3a population that is rearranging the Tcrb locus prior to β-selection [86]. Further, among the DPs, mostly pre-selection DP cells, but not post-selection DP cells, proliferate, and only a small fraction of CD4SP and CD8SP cells. Therefore, proliferation would mainly stop before the post-selection DP phase and partially restart in the late stages of single positive populations.

Altogether, these single-labelling strategies are an indirect way to observe a wave of labelled cells but do not directly capture the details of proliferation (how many divisions, synchronous, and percent of cells dividing). Further, the dilution of signal along with the divisions in the SP stage, as well as the increase in the frequency of labelled cells by division of two half-labelled daughter cells can make the interpretation of results tedious and require mathematical modelling to extract cell cycle parameters, as done in [87] for population turnover.

Preprints (www.preprints.org) | NOT PEER-REVIEWED | Posted: 19 January 2021 doi:10.20944/preprints202101.0388.v1

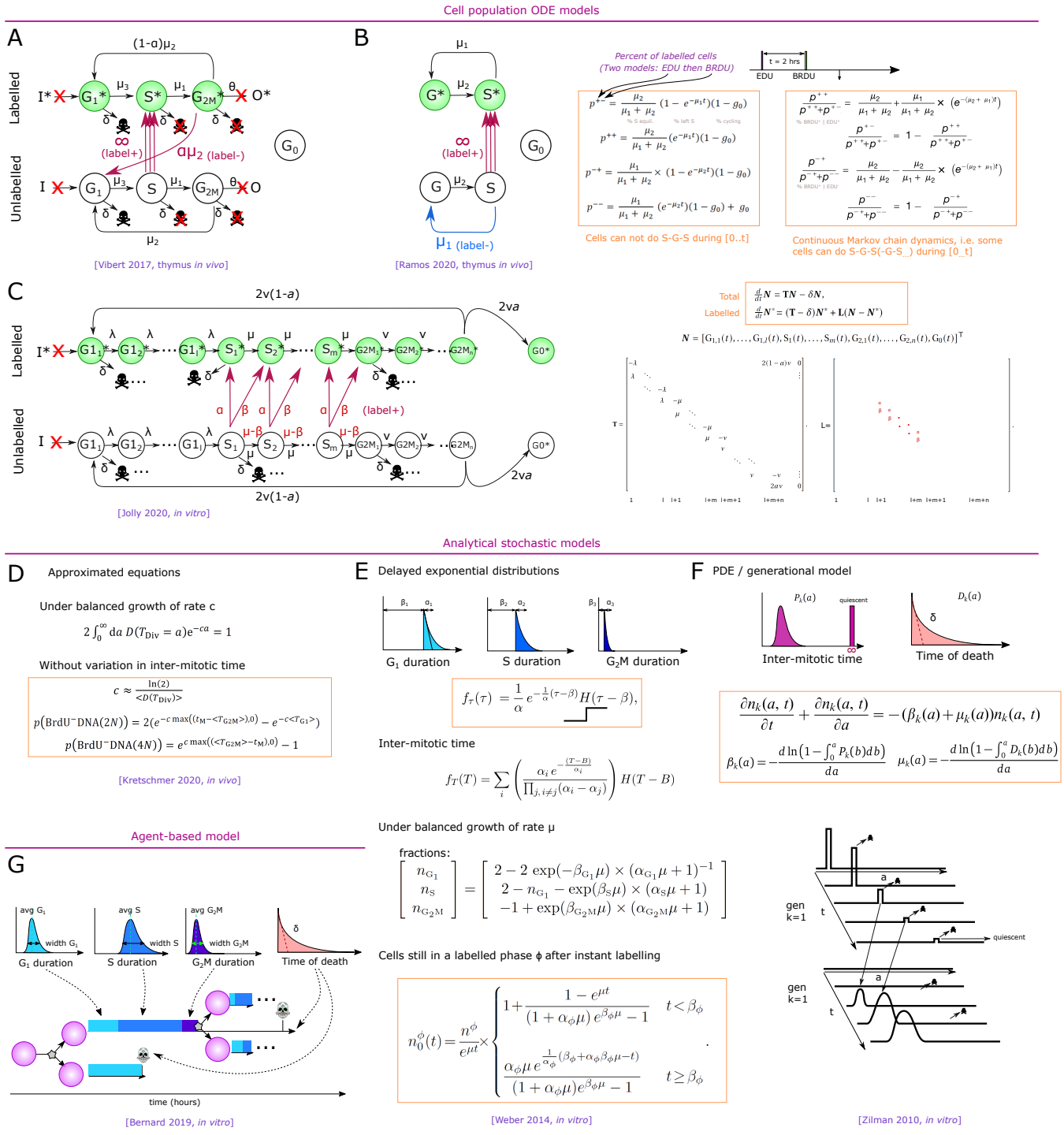

Figure 4. Mathematical approaches used to infer proliferation speed. (**a-c**) ODE-based models for simulating *in vivo* labelling of cells. Such models typically model an instant labelling of all cells in S phase, and possibly a decay of the labelling by proliferation (in (**a**) only). In (**b**), a two-pulse labelling is applied and the dynamics of labelling are simulated for both labels. Assuming instant labelling of all cells in S phase, the first labelling stains the equilibrium value of such cells. Two strategies lead to different analytical formula: assuming the labelling interval t is negligible compared to the cell cycle, cells cannot return in S; or simulating a 2-states markov chain for the state of the cells at second labelling allows some cells to cycle multiple times. In (**c**), the ODEs can be represented with a matrix formalism. (**d**) From mean field equations of growing populations, assuming a certain synchrony of the total cycle, the state of initially labelled cells over time can be predicted. (**e-f**): Stochastic models for cell proliferation with time-distribution of each cycle phase under exponential growth, assuming delayed exponential distributions (**e**) or with generic cycle and death times convenient when using gamma distributions (**f**). (**g**) Agent-based explicit simulation of each event at the cellular level, predefined from time distributions.

Preprints (www.preprints.org) | NOT PEER-REVIEWED | Posted: 19 January 2021 doi:10.20944/preprints202101.0388.v1

3.2.2. One-point EdU or BrdU pulse followed by DNA staining at different time points

This approach allows to track the fate or cycle phase of cells that were in the S phase during the pulse at later time-points (Figure 3C). The study by Baron et al. followed the percent of $BrdU^+$ cells after a single pulse labelling *in vivo*, in the full thymus [88]. They observe that DNA amounts linearly increase with time among $BrdU^+$ cells. By linearly estimating the time to reach the highest DNA amounts (4N at G2), they estimated that the S phase would be around 6.5 hours. This approach implies to take an average DNA content of all cells in S phase to 3N, because a single BrdU pulse does not allow for the determination of the precise onset of DNA replication in individual cells. By following when $BrdU^+$ cells return to the G1 and to the S phase, they concluded that the G1 duration would be around 10 hours while the G2M phase would be of 1.5 hours resulting in a full cycle of around 18 hours (Figure 3C). Such a fast cycle would be consistent with the fast reconstitution of the thymus after transient atrophy for instance. Since the authors used all thymocytes without gating sub-populations, the results of this study most likely reflect an average behavior among the largest populations of proliferating cells.

Vibert et al. [89] developed a staining protocol, with a first set of 2 pulses of EdU intravenous injections one hour apart, followed by a third EdU pulse 14 hours later just before a unique time-point of harvesting the cells, aiming at labelling more cells among slowly proliferating populations *in vivo*. At the time of measurement, the authors additionally stained for DNA content to separate the G0/G1, S and G2 phases together with the EdU labelling. They analyzed in that way three populations: i) EdU^+ cells, i.e., all the cells that were in S phase during at least one pulse. ii) Cells in G0/G1 that were not in the S phase during the labellings "G0/G1 EdU^-", and iii) cells in G2/M that were not in the S phase during one of the labellings. They measured aged and young mice of two different backgrounds, for the main populations including separated DN1 to DN4 populations. They built an ODE model for each population with 6 compartments: 'G0/G1', 'S' and 'G2M', each EdU labelled or unlabelled (Figure 4A), and simulated the experimental set-up with instant labelling of the cells in the S phase at the three time-points of the pulses. They inferred the parameters of the model (speed of transfer from each compartment to the next) by fitting the simulations to the three populations at the final time-point of measurement. Obviously, fitting 6 parameters to 3 observed variables at one time-point per compartment was not feasible so the authors took realistic assumptions to reduce the system down to 2 parameters, by limiting death to the G0/G1 stage, by fixing the S phase to 6.5 hours from literature [88] (although this value might not apply to all populations), and by neglecting the inflow/outflow of cells from upstream populations during the 16 hours of the experiment. This approach raised values of G0/G1 duration from typically 2.5 to 12 days for proliferating populations, while non-proliferating populations like $CD44^{low}$CD4SP or CD8SP reached more than 300 days cell cycle (probably an artifact indicating that most of them do not cycle at all). They also observed a lower frequency of labelled cells in 18-month old mice compared to young mice, consistent with literature [48], and interpreted the results as shorter cell cycle times in younger mice. The inferred cell cycle durations by Vibert's model [89] are longer in comparison with above mentioned *in vitro* proliferation assays that suggested at least one division per day along DN and early DP stages. Although the model equations were validated by recapitulating the single pulse BrdU kinetics from the study by Baron et al. [88] along a few hours, several factors might need to be accounted for, due to the 14 hours period between pulses in [89]. First, some cells could actually have been in two consecutive S phases at first and last labelling (i.e. performing G2, M, G1 and returning into the S phase during the 14 hours interval). For the SP populations, bystander non-proliferating cells could help interpreting the low percent of labelling. Finally, there is a possibility that labelled cells from highly proliferating early DP cells could contaminate the late DP compartment that has a shrinking dynamics due to high

Preprints (www.preprints.org) | NOT PEER-REVIEWED | Posted: 19 January 2021 doi:10.20944/preprints202101.0388.v1

death (i.e. recently arriving cells can occupy a high percent of late DPs at steady state). Finally, the G2/M EdU$^-$ population is supposed to be very minor because most cells at G2M at the measuring time-point were in S phase just before (during the last pulse), which can generate noise in the parameter fitting. Altogether, albeit labelling more cells, this time-extended experimental setting seemed to generate new layers of complexity in interpreting the labelling results, that might require a more complex model design. This example illustrates the complexity of matching a theoretical model with a practical experimental setup.

3.2.3. Dual labelling with EdU and BrdU at different time-points

This technique allows to differentially label the cells entering or leaving the cell cycle, and to follow their cycle phase over time (Figure 3D). For instance, with 1 hour difference between EdU and BrdU pulses, this technique has the power to mark synchronized cells entering or leaving S phase at a given interval, and could reveal heterogeneity in the S or G1 phase durations. Thus, Ramos et al. employed such a system to determine alterations in cell cycle duration of the DN2 and early DN3 compartments suggested to serve as sensors for DP thymocyte cellularity [69]. At an excess of DP cells in an experimental model of cellular competition, DN2 cells incorporated less EdU, suggesting that higher amounts of DP thymocytes slowed down the cell cycle of DN2 cells. They then used the EdU / BrdU dual pulse experiment to build a linear ODE model for cells in S or G phase, labelled or not labelled (Figure 4B), constituting a simplified version of Vibert's model [89] (Figure 4A). After an EdU pulse, followed by a BrdU pulse at 2 hours and harvesting the cells at 4 hours, they fit the model with the amount of cells in each quadrant.

Using a continuous Markov chain model (Figure 4B, right equation), taking into account that some cells can leave and re-enter the S phase during the time of labelling (2 hours) while other cells would be extremely slow (which is a consequence of assuming exponential residence time in each compartment), DN2 cells were estimated to have a total cell cycle duration of 9 hours at normal DP thymocyte cellularity as compared to 15 hours in the presence of excess DP thymocytes [69]. This model was useful in comparing the cycling behavior of cells in two environments (for which the EdU/BrdU labelling were already indicative, but additionally providing an estimate of the difference in cell-cycle duration). Notably, an earlier model, assuming that labelled cells cannot return to S phase during the 4 hours of staining, inferred very short cell cycle durations in the range of 3 to 4 hours from the same data (Figure 4B, left equation) [90]). This example highlights the impact of model design on the inferred cycle duration values, and underscores that single linear ODEs generate an exponential residence time of cells at each stage, requiring some care in model design or interpretation.

Jolly et al. [91] have proposed an ODE-based model that solves this problem (Figure 4C) by separating each cycle phase into many sequential steps, and applied it on a EdU labelling kinetics scheme in cell cultures, and that would also be valid for dual pulse. Due to the complexity of the model, an analytical solution for the dynamics of labelling is not easily available, and a fitting procedure to experimental datasets allows to infer the cell cycle duration. The equations can conveniently be represented as matrix multiplication and the authors propose an analytical formula linking the frequency of cells expected in each cycle phase with the population parameters assuming steady state growth (also called balanced growth). This approach allows for a reduction of the parameter space or validation of predictions by comparing predicted proportions in each phase to experimental results.

Preprints (www.preprints.org) | NOT PEER-REVIEWED | Posted: 19 January 2021 doi:10.20944/preprints202101.0388.v1

3.3. Future models and finding the optimal experimental set-up

The models described above were only partially successful in extracting robust durations of the cell cycle. This might be due to limitations of the datasets that might not contain the appropriate time-points or due to the assumptions of the modelling strategies. One also needs to take into account that the models cannot have more degrees of freedom than the complexity of the datasets to avoid overfitting. Combining all approaches described above a EdU/BrdU dual pulse coupled with DNA labelling at multiple time-points may solve some of these issues [92]. Other modelling approaches could be successful in extracting thymocyte proliferation rates, and in particular how to link the single cell proliferative behavior to the observed population parameters at the higher scale. Stochastic models for cell division based on time distribution of events seem most suitable for this task.

Recently, Kretschmer et al. [93] studied the cell cycle duration of memory T-cell precursors and effector cells *in vivo* using the dual EdU/BrdU labelling strategy. Assuming an exponentially growing population, they approximate the relation between the growth rate and the average division time assuming it has no standard deviation. They also derived an approximated mean-field formula of the stochastic model for the amount of cells that divided and re-entered the G1 phase (Figure 4D).

In [94], the authors derived analytical formulas for the fate of labelled cells through their progression along the cell cycle. They used a stochastic model where each cycle phase duration follows a delayed exponential distribution (Figure 4E). The authors assumed a 'balanced exponential growth' of the population without death, i.e. cells are growing with apparent rate μ (curve proportional to $\exp \mu t$), and kept a constant fraction of cells in each phase over time. The type of chosen time-distribution can allow for analytical formulation. Starting from a pool of labelled cells in S phase (just after BrdU), such cells that entered G2M after a time t can be separated as cells of all possible 'age' a within G2M and therefore the corresponding time δ they took before exiting the S phase since the beginning of (instant) labelling, such that $a + \delta = t$. This is actually a convolution, and using a Laplace transform of the delayed exponential distributions yields an analytical formula for the dynamics of labelled cells either remaining in the initial S phase (Figure 4E, low formula), or progressing to the next phases. Further, the authors provide a formula relating the expansion rate μ to the phase parameters α_i and β_i and the ratio of cells in phase G1, S and G2M: n_1, n_2 and n_3 (Figure 4E, medium formula). They predict that the dynamics of labelled cells from any phase ϕ that progressed to the next phases typically follow two steps: a first period, of duration β_ϕ where labelled cells exit the initial population with a constant speed, followed by a period where the very last labelled cells exit, revealing the exponential decay part of the S phase duration distribution. The authors show that the initial derivative of the curve requires two early experimental points and is enough to set the expansion rate and some alpha parameters, while a third experimental data point is needed after $t = \beta_\phi$ to identify the average duration of the exponential decay. This approach therefore seems suitable to interpret *in vivo* thymocyte EdU/BrdU labelling, with the limitation that the third optimal experimental time-point is difficult to estimate because it needs a pre-existing guess on after how long the cells in S phase start to leave (time β_ϕ), and the exponential decay might be very short. Since the model has been designed for cells growing in culture, it is yet to be determined whether the hypotheses of no death and balanced growth would still be valid *in vivo* where cells can exit a compartment, potentially after a regulated number of divisions.

Preprints (www.preprints.org) | NOT PEER-REVIEWED | Posted: 19 January 2021 doi:10.20944/preprints202101.0388.v1

Zilman et al. [95] proposed a more general stochastic model including a distribution of inter-mitotic time (cell cycle completion) and death, derived from the von Voerster equation [96], which relates the amount of cells and their age within a population as a partial differential equation. More precisely, the distribution of the age of cells within each generation is stored, and evolved at each time-point. The fate of the cells at the next time-point is a convolution of cells at each age and the distribution of time inside this generation (inter-mitotic time) or death. Again, a Laplace transform becomes convenient because it transforms the convolutions into multiplications (Figure 4F). The authors derive analytical formula for the dynamics of a pool of labelled cells and reproduced quite well experimental datasets using labelled dye dilution *in vitro*. They show that the gamma distribution ia a good approximation to the lognormal distribution, whose transform is too complex [97]. The authors also adapt their formula to branching imbalanced divisions allowing to introduce asymmetric divisions.

Altogether, it is likely that a combination of Weber et al. approach [94] with the generational model of Zilman et al. [95] including death could allow to derive analytical formulas for BrdU or EdU labellings that fit with synchronized proliferation with a fixed number of divisions in the thymus and be used for *in vivo* experimental datasets.

A last and most general strategy is the explicit simulation of the stochastic equations using an agent-based model with thousands of cells with an associated distribution of time for each event (Figure 4G), as done for 2D tumor tissue cell cycle in [98]. Each cycle phase can follow a lognormal distribution (like in the cyton model [99,100], and death can be drawn as an exponential distribution, or could be restricted to the G1 phase for instance. It becomes easy to simulate the exact experimental setting.

Future technical development might guide the design of new types of models, such as for the interpretation of Ki67 expression [101,102] and its degradation at specific cycle phases. The measurement of TREC recombination circles dilution from TCR recombination is an indirect read-out for proliferation and population dynamics that has been leveraged using mathematical modelling [103] and is suitable for analyzing human samples as well as the use of labelled deuterium in drinking water [104]. Finally, newly developed *in vivo* reporters for cell cycle might allow more precise longitudinal evaluation of cell cycle over time [105].

4. Estimation of *in vivo* cell death in the thymus

Estimating the rates of thymic selection is critical for the calibration of mathematical models of T-cell developmental dynamics. However, cell death is particularly hard to visualize *in vivo* and macrophages can remove thymocytes extremely fast and even seem to contribute to inducing cell death [106]. Experimental approaches to determine the extent of thymic selection, sometimes combined with mathematical modelling, have been reviewed in [12]. We provide a brief overview here, illustrating some key experimental constraints. Of note, depending on the study, the 'efficiency of selection' can be estimated either as flow of cells dying per day at a certain stage (rate), or as the amount of cells that will die or survive through selection from a defined pool of cells (percent). The latter definition depends on the residency time of cells at different stages, which is also hard to measure for heterogeneous populations. A number of early studies estimated rates of selection by either directly inducing negative selection [107] or removing selecting ligands (i.e. MHC) from a variety of thymic APCs to induce failure of positive or negative [108–111]. Together, these studies yielded a broad range of frequencies of death by neglect or clonal deletion. However, interpreting these data is difficult, as removal of MHC removes both positively and negatively selecting signals and negative selection in particular is likely to occur over prolonged periods of time, ranging from DP thymocytes that have just completed Tcra rearrangement to SP thymocytes, as well as

Preprints (www.preprints.org) | NOT PEER-REVIEWED | Posted: 19 January 2021 doi:10.20944/preprints202101.0388.v1

upon interaction with more than a single type of thymic APC. Another approach was based on continuous BrdU labelling using transgenic T cells with CD4 or CD8- biased TCRs that were known to survive positive selection [112]. The aim was to monitor the maximum number of cells that could survive through positive selection *in vivo* by filling the thymus by survivable TCRs and compare this number to that of surviving cells in the WT setting. This study suggested that at least 40% CD8 TCRs and 90% CD4 TCRs are removed through both positive and selection combined.

Two more recent studies have revisited the death estimations using more direct, signaling reporters. Stritesky et al. used a $Nur77^{GFP}$ reporter to quantify levels of TCR signaling in thymocytes [34], comparing WT or Bim-deficient mice, in which negatively selected thymocytes fail to undergo apoptosis. The authors distinguished three populations based on GFP reporter expression: GFP low cells that die by neglect (positive selection), GFP intermediate cells that have received a positively selecting TCR signal, but may still audit for negative selection, and finally GFP high cells that are deleted in WT mice but persist in $Bim^{-/-}$ cells. Following the observation that $Bim^{-/-}$ cells spend longer in the SP4/SP8 compartment than WT cells on average, they estimated that, at the scale of a 200-250 million cells per thymus, 3 million cells survive both positive and selection per day, while 16,7 million cells would die by negative selection. A minor caveat for determining exact rates of selection stems from the observation that $Bim^{-/-}$ thymocytes have an increased residence time when compared to WT cells in the SP compartment, because they do not die and are kept longer in the thymus. However, $Bim^{-/-}$ cells comprise both GFP intermediate positively selected cells, which should exit normally as WT cells, as well as GFP high cells, which are indeed staying longer. As raised by Yates [12], dying cells and surviving cells have a different residence time (even if following the same mechanism). This means that extra $Bim^{-/-}$ cells that "should have died" stayed actually longer than the average residence time of all $Bim^{-/-}$ cells, and negative selection could therefore be slightly lower than estimated.

Daley et al. [113] used a similar approach based on accumulation of cells poised for clonal deletion in $Bim^{-/-}$ mice in combination with a dual transgenic TCR/cognate antigen model. Expression of self-antigen deleted 60% of the CD4 SP cells compared to mice without expression, while in $Bim^{-/-}$ cells, those cells survived. The authors identified Helios as a surrogate marker for cells undergoing negative selection. Using this marker in combination with markers of progressive thymocyte maturation, they proposed a multi-step model of clonal deletion, concluding that negative selection deletes 55% of the positively selected thymocytes already in early SP cells.

Finally, some population models described above, such as those developed by Sinclair et al. [44] or Thomas-Vaslin et al. [54] inferred death rates from their experimental datasets, but from populations lacking proliferation. This means the inferred rates are actually including the effect of proliferation, and could be re-estimated based on proliferation studies. Sinclair estimated that 75% of cells fail positive selection and only 2 to 5 percent of cells become CD8 and CD4 at the end, respectively. Including proliferation at SP stage would actually mean that more cells died by negative selection, probably not that far away. In Thomas-Vaslin's model, where cells can die only at the DP stage, 97.5% of the pre-selection cells die at that stage.

Taken together all studies converge on a very high frequency of death through selection, between 90 to 97.5%, which could be even higher when including proliferation. However, it remains a challenge to fully disentangle the contribution of death by neglect vs. clonal deletion as well as the type of APC, onto this death load. In conclusion, a thorough comparison of experimental datasets ranging from signaling reporters, dynamical datasets (like recovery after atrophy), and EdU/BrdU labelling into a single mathematical analysis could narrow down the selection rates with better understanding on the experimental perturbation biases, yet is very tedious.

Preprints (www.preprints.org) | NOT PEER-REVIEWED | Posted: 19 January 2021 doi:10.20944/preprints202101.0388.v1

5. Multiscale considerations on thymic dynamics

Selection processes in the thymus constitute quality control mechanisms downstream of the bona fide random somatic recombination of TCR genes into a functional but not self-reactive repertoire. Thymic selection emerges from events at the molecular and cellular level (Figure 5A). Understanding how the dynamics of T-cell development arise from these lower scales requires multiscale modelling.

At the molecular (and genetic) scale, virtually each thymocyte that completed the pre-selection DP stage, carries a different somatically recombined TCR, composed of one TCRα chain and one TCRβ chain at its surface. Lack of allelic exclusion of the Tcra locus allows for the generation of T cells with two distinct TCRs. APCs display a subsampling of possible self-peptides on their surface MHC complexes. Binding between TCR complexes and pMHC complexes triggers TCR signaling on the thymocyte. The landscape of self-antigens presented in the thymus is particularly complex as it depends on the type of APC, their capacity to express many proteins from the genome, distinct mechanisms of antigen processing, and the structure of the 6 MHC proteins encoded by highly polymorphic genes.

At the cellular level, thymocytes move and sequentially interact with APCs. The multiple pMHC complexes and TCRs of the APC and thymocyte, respectively, located in the membrane cell-cell contact, have the possibility to interact. The affinity (existence of high affinity binding) as well as the avidity (amount of binding TCR-pMHC couples) is translated into TCR signaling that is integrated between cellular contacts.

At the physiological level, the outcome of thymic selection is defined by successful recognition of foreign peptides (antigens) in the context of self-MHC, resulting in T cell activation. Cells whose TCR form high-affinity interactions with self-peptide loaded MHC on APCs in the thymus die in the process of negative selection. It is not fully clear how positive and negative selections are decided, depending on the TCR affinity, TCR cross-reactivity to different self-peptides, and the avidity of sequential cellular interactions, through TCR signaling [11,114]. Finally, the boundary between negative selection and Treg cell differentiation is unclear as both Tregs and Tconvs surviving thymic selection share some identical TCRs (see the overview of Klein et al. [72] for a review on Treg differentiation models). Several multi-scale mathematical models predicted the properties of the produced TCR repertoire due to positive and negative selection, based on a static set of TCRs and MHCs. These models, comprehensively reviewed in [12], have been helpful in particular to understand trade-offs between TCR cross-reactivity, pathogen recognition and auto-immunity; the induction of MHC recognition, restriction or Treg differentiation from positive and negative affinity selection thresholds; or how thymic selection generates holes in the repertoire for pathogen coverage. Very few models however have investigated how thymus dynamics arise from the lower scale of single cell motility and fate decision, and how it affects the higher scale of repertoire generation and TCR clonality.

Preprints (www.preprints.org) | NOT PEER-REVIEWED | Posted: 19 January 2021 doi:10.20944/preprints202101.0388.v1

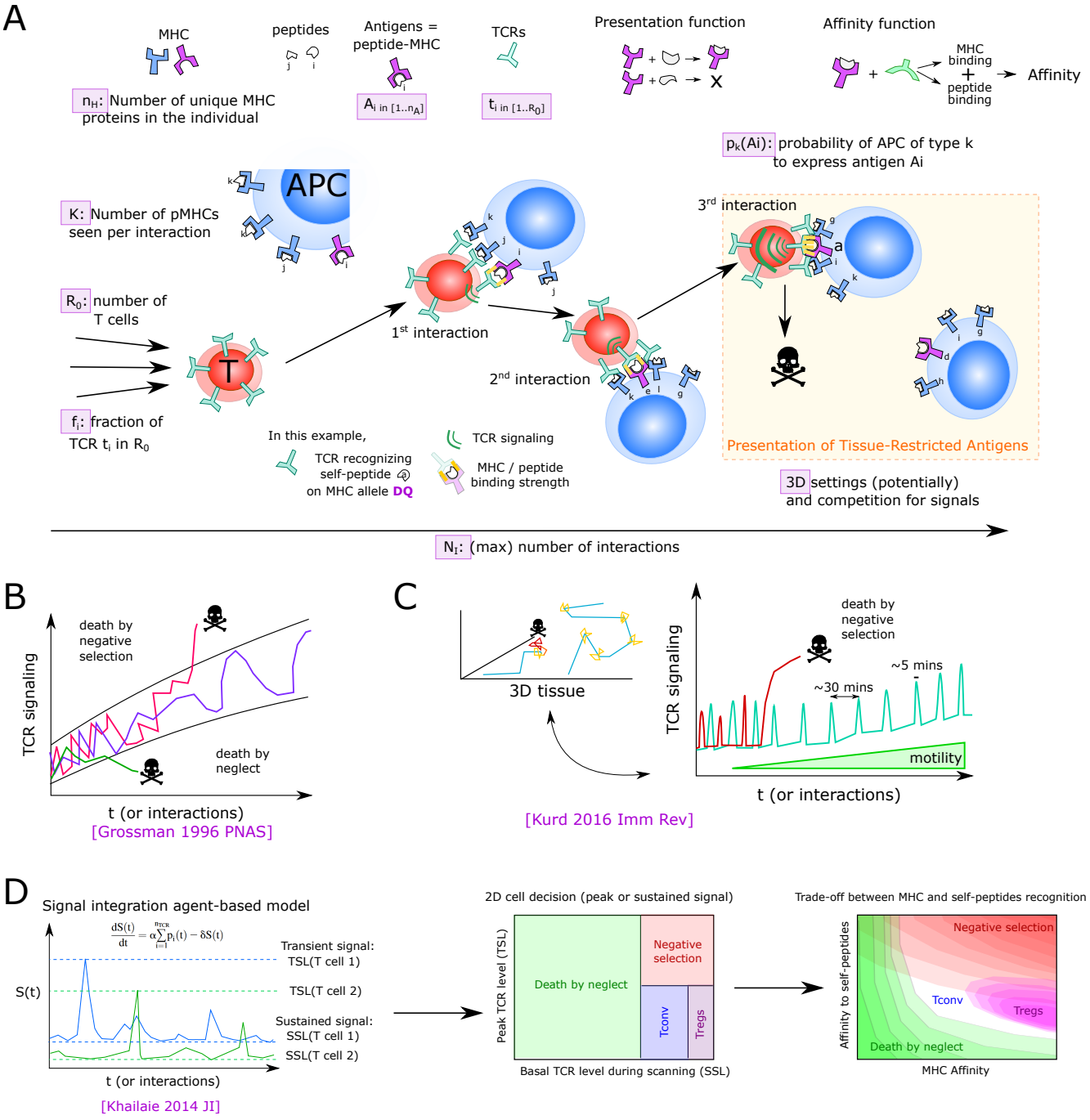

Figure 5. Different biological scales underlying thymic selection and models linking cellular interactions to signal and fate. (**a**) TCR signaling, and thereby thymic selection fate, is mediated by the encounter with Antigen Presenting Cells (APCs) displaying samples of self-peptides on their MHCs. TCR signaling can be induced by high affinity to a MHC (typically at each interaction), or to a cognate peptide (more rarely). Specific types of APCs express a larger scale of self-antigens (Tissue Restricted Antigens) and are compartmentalized in space (yellow box). (**b**) Model predicting that T cells would show increasing signal over time due to increased TCR expression, and suggesting two self-adapting thresholds, for positive and negative selections. (**c**) Experimental observations on ex-vivo thymic slices, where T cells migrate and get signaling at each APC encounter. The encounter with cognate peptide leads to stop and strong signaling, while non-self-reactive interactions are shorter. D. Signal integration model. Each encounter with APCs leads to a transient increase in the integrated TCR signaling depending on the affinity (or avidity) of TCR-pMHC binding at each cell interaction. The integrated signal is translated into peak signal (Transient Signaling Level, TSL) and basal signal (Sustained Signaling Level, SSL), used by the T cells to decide their fate. Due to the correlation of SSL with MHC affinity and TSL with highest self-peptide affinity, the decision translates into Tconv with intermediate affinity to MHC while Tregs emerge with higher MHC affinity.

Preprints (www.preprints.org) | NOT PEER-REVIEWED | Posted: 19 January 2021 doi:10.20944/preprints202101.0388.v1

5.1. Linking the history of TCR signaling to cell fate

Several studies have proposed to link the dynamics of TCR signaling to thymic selection processes, which would constitute suitable bases to simulate thymus dynamics in the future:

First, Grosmann et al. [115] proposed a theory on how the dynamics of TCR signaling could look like, and how it could be translated into positive or selection decisions (Figure 5B). Based on the observation that TCR expression and signaling gradually increase over the DP stage the authors proposed that T cells maintain two tunable activation thresholds: a lowest signaling level threshold to survive positive selection, and a higher threshold to delineate deletion by negative selection, and that both thresholds would adapt to each other or to the current signal level. They defined a variability-maintenance threshold that grows together with the expression of TCRs at the surface, and an activation threshold, linked to the former threshold, relatively higher than the maintenance threshold, for negative selection. This theory can explain that DP and SP cells have different activation thresholds, and allows T cells to self-tune their signaling thresholds to their environment (antigen expression pattern), possibly giving a robust response independently of a constant inflammatory context or perturbation. A large body of evidence has detected quantitative and qualitative differences in the TCR signaling leading to positive or negative selection [6–10]. Kurd et al. [116] and a series of papers from Ellen Robey's lab [117–119] could directly visualize the temporal signals received by thymocytes during positive and negative selection, thanks to *ex vivo* calcium imaging of thymic slices (Figure 5C). Basal signaling was observed, composed of peaks of typically 5 mins interspersed by 25 minutes of resting, matching patterns of stop and migration, while encounter of cognate ligand lead to pronounced arrest and elevated levels of sustained signaling, eventually resulting in cell death. The observation that positive selection happened in *ex vivo* 3D slices but not in *in vitro* cultures [116], support the hypothesis that transient regularly interspersed signals are required for proper signal-to-fate decisions. It is plausble that a cell needs to regularly detach from one APC to the next to avoid strong signaling. This is a rare study linking calcium signaling to changes in motility suggesting that the patterns of T-cell search are also impacted by TCR signaling and could benefit from a modelling on their own.

An agent-based model has been developed by Khailaie et al [120] (Figure 5D) to link cell-cell interactions with single cell TCR signal integration, using string models for TCR-pMHC affinity with short range positional correlations. In this model, a list of T cells with random TCRs sequentially interact with APCs carrying a random sampling of pre-defined self-peptides at each time-point, all presented on the same MHC molecule, and a TCR signal is integrated over time at each interaction with a decay rate. This leads to peaks due to encounter with higher affinity peptides with a constant contribution of the MHC at each interaction. Similar to the studies of Grossman et al. [115] and Kurd et al. [116], the authors proposed to use a threshold on the basal signaling level of a thymocyte as a decision to survive positive selection, while a threshold on the highest peak would define autoreactivity of a TCR. Khailaie also noted a trade-off for selected cells between sustained and peak signaling (cells with higher basal peak would die when they encounter a medium affinity peptide while low basal peak would allow to bind peptides with higher affinity and survive), and suggested that Treg cells are more affine to MHC, that would endorse them with higher cross-reactivity.

Recognition of self-peptides plays a substantial role in positive selection [121–124], but their relative abundance is heterogeneous [125]. It is tempting to propose that frequent or groups of structurally similar antigens could generate a signal supporting positive selection of TCRs recognizing them with medium affinity, while rare antigens would not have this capacity. It would be interesting to check whether this happens in Khailaie's model using a mixture of frequent (possibly similar) antigens and more

Preprints (www.preprints.org) | NOT PEER-REVIEWED | Posted: 19 January 2021 doi:10.20944/preprints202101.0388.v1

rare antigens, and correlating cell fate with affinity to these frequent antigens instead of MHC affinity.

Although the link between basal and peak signaling into positive and negative selections is still speculative, different signaling pathways have been associated with both selections and Treg cell development (for instance ERK and Ras signaling [9,10]). It is tempting to hypothesize that different pathways could behave as band-pass filters, with some 'fast' pathways getting activated by rare but strong encounters (peak signal) and other pathways slowly activated after many repeated interactions [6]. For instance, an ODE-based model for TCR signaling has been predicted to be able to discriminate self and foreign peptides [126] based on interaction frequency. More generally, in the context of frequential inputs, a Fourier transform of TCR signaling models could help predicting the signal properties required for different fate decisions.

Together, these studies support the notion that positive and negative selection could be mechanistically defined by different types of signaling, in which a rapid, high peak promotes negative selection while basal signaling defines positive selection. Notably, the experimentally observed signals were in almost perfect agreement to those predicted by [115]. Further, these models are suitable to simulate developmental dynamics at the DP and SP stage from single cell encounters, although at present these models cannot yet incorporate a possible interdependence between TCR signaling and a cell's decision to proliferate at the early DP or late SP stages. In contrast to single cell models, dynamical models presented in section 1 encoded differentiation (to CD4SP, CD8SP or Treg cells) as a constant rate, thus masking potential regulatory mechanisms that agent-based models would intrinsically include. For instance, Kurd et al. [116] suggested that mismatched CD4SP or CD8SP with a TCR that recognizes the 'wrong' MHC would not get sustained signaling in the SP stage, and die by neglect, showing that signal integration is likely also important for CD4 vs. CD8 differentiation dynamics.

5.2. 3D models of thymic development, APC types and antigen spatial compartmentalization

T-cell development is coupled with regulated migration patterns. ETPs enter at the cortico-medullary junction from blood vessels, and both DN and DP development happen inside the cortex, where cTEC and other APCs support positive and negative selection of DPs. The maturation of DPs into SP is associated with changes in chemokine receptors and migration towards the medulla that occur typically 12 to 24 hours after the onset of positive selection [116]. CD4 and CD8 T cells downregulate the opposing coreceptor with different timing, later for CD8 SP cells. In the medulla, AIRE-expressing mTECs show a larger panel of antigens referred to as tissue restricted antigens (TRAs), while other APCs (dendritic cells (DCs), B cells, stromal cells [127]) can also present self-antigens, or antigens captured in the periphery by migratory DCs [72,128,129]. For instance, DCs seem to be more efficient at mediating negative selection in the cortex while cTECs are also presenting self peptides. Rare DCs are located close to capillaries and surrounded by CCL21. Interestingly, DCs and mTECs as well as vascularization are much denser at the cortico-medullary interface, suggesting its crossing has the highest strength of selection (or avidity) [72]. The molecular cues guiding the transit of thymocytes from cortex to medulla are poorly understood. While it is well established that chemokine receptors CCR7 and CCR4 play dominant roles in this process, it has recently been suggested that these receptors indirectly promote spatial organization of thymocytes by organizing the localization of thymic APCs, in particular DCs, and mediating their interaction with thymocytes [130,131]. As a consequence, loss of either chemokine receptor results in defects in central tolerance [131,132]. Notably, the presence of a thymic medulla is critical for development Treg, but not Tconv, cells [59]. The egress of T cells is mediated by the S1P1 receptor, which is upregulated only at the latest stage of SP maturation. Treg cells are believed to stay longer in the thymus, and different

Preprints (www.preprints.org) | NOT PEER-REVIEWED | Posted: 19 January 2021 doi:10.20944/preprints202101.0388.v1

types of APCs harbor different Treg inducing capacity [133]. It has been suggested that certain antigens could be expressed in spatial niches, added to the fact that TRAs are preferentially expressed in the cortico-medullary junction [72]. These arguments support the notion that the spatial organization of the thymus is critical for its function and would call for spatial mathematical models.

So far, only a few models have attempted to simulate the thymus in 2D or 3D. Elfroni et al. [134] developed a framework able to simulate motility, chemokine sensitivity, proliferation and death on a 2D lattice system, similar to later developed platforms like Morpheus [135], and including the cortex and medulla. The model was used to recapitulate the migration of cells following chemokine gradients [136], in the context of WT versus CCR9-deficient mice. They also measured an effect of space competition into apoptosis and the subsequent amounts of generated CD4 and CD8 T cells. Further, the cell-cell contact dissociation rates impacted the CD4 to CD8 decision. Souza-e-Silva et al. [137] used a simpler mathematical formalism and simulated chemokine levels and cell decisions as a cellular automata, i.e. a 2D grid, where each position can only have predefined states that are updated according to the neighboring states. Interestingly, the authors could reproduce realistic movement between cortex and medulla, and proper dynamics of development and residence times from a few cells to a full thymus at equilibrium. They could modulate the T-cell dynamics from changing the properties of the epithelial network. The fact that correct dynamics can emerge from simple 2D models makes it tempting to believe that it will soon be possible to incorporate multi-scale models in a 3D setting, incorporating data on migration from thymic slices, proliferation, population dynamics and signal integration. The findings that thymocyte migration and signals are correlated [116] would suggest to use such models to calculate a signal integration and fate decision from the interactions like [138,139], feeding back to a modulated searching behavior of the cells.

5.3. Thymus dynamical models can help the analysis of TCR repertoires

High throughput sequencing has provided in-depth information on TCR diversity generated in the thymus [140]. Dynamical models of T-cell development are likely to help understand the formation of pre-selection repertoires and their shaping through selection.

For instance, a mathematical model has been developed to simulate V(D)J recombination of the Tcra or Tcrb gene [141]. This tool takes a repertoire and proposes the most likely V(D)J recombination event for each sequence by inferring probabilities of using each V, D or J segment (called recombination parameters), including deletion and insertion events. Then, from inferred recombination parameters, it becomes possible to generate new TCR sequences following the same recombination model. While this model has been used to analyze peripheral TCR repertoires, it actually simulates Tcrb recombination before the DN3b stage or Tcra recombination during the DP stage, which are impacted by both thymic selection and population dynamics. An example in Figure 6 demonstrates that proliferation can strongly alter the relative frequency of clones in the periphery. We speculate that, using knowledge or models on thymus population dynamics, new recombination models could be designed, which include variation in clonal expansion for the analysis or generation of TCR repertoires. Further, such models comparing pre-selection and post-selection repertoires could identify which TCR sequences are preferentially deleted or expanded.

Moreover, the patterns of thymocyte clonal expansion are poorly described and it is not clear whether T cells are selected independent from each other, and to which extent there is competition between antigen-specific clones, or how the competition for cytokine signals determines terminal differentiation. Newly developed *in vivo* barcoding

Preprints (www.preprints.org) | NOT PEER-REVIEWED | Posted: 19 January 2021 doi:10.20944/preprints202101.0388.v1

approaches coupled with statistical analyses are suitable to follow the clonality of progenitors along thymic selection [142]. Such datasets will likely support the development of lineage tree algorithms possibly combined with population dynamics and branching fate decisions in the thymus. In turn, this could provide valuable information on the relative clonal expansion in DP and SP stages to simulate proper population dynamics.

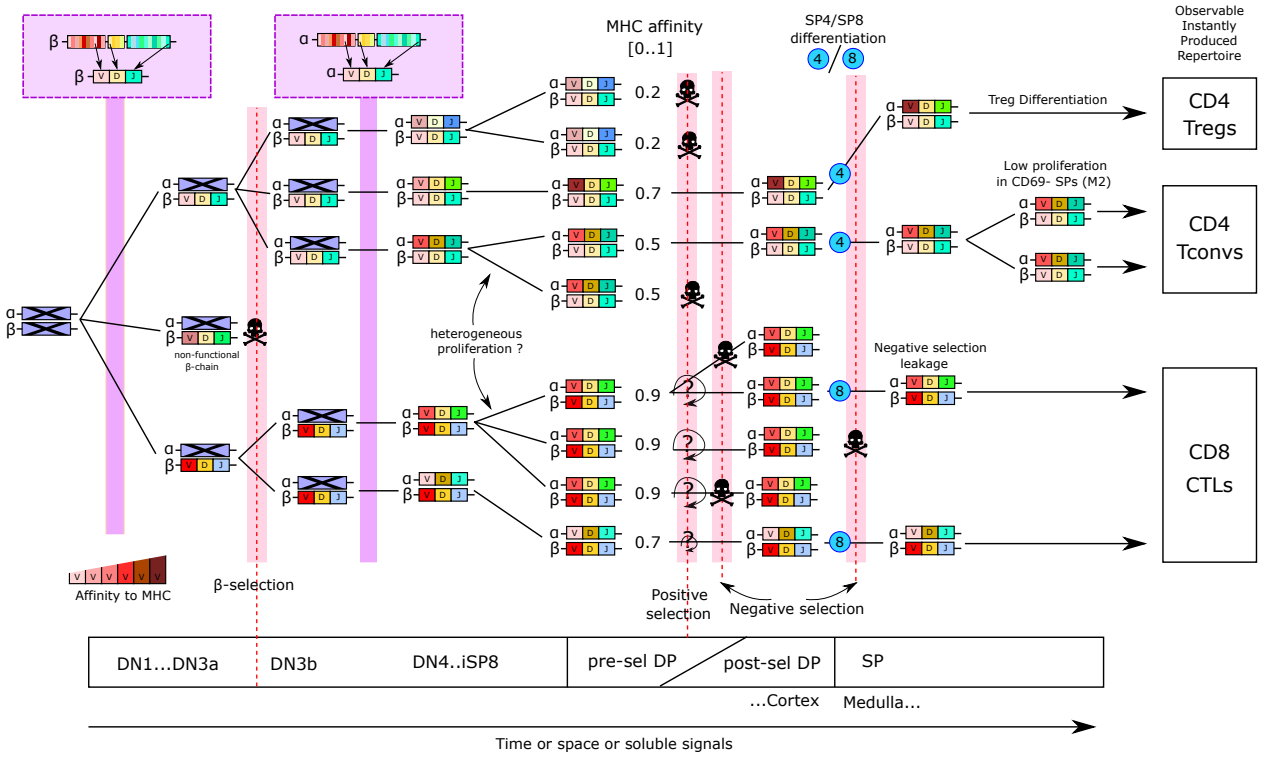

Figure 6. Cross-talk between recombination probabilities, proliferation and selection on the observed TCR frequencies in the repertoire, suggesting that the mechanistic recombination events and the frequencies of TCRs with a recombination scenario might not directly be equal and need more mathematical investigation.

5.4. Future types of multiscale models

New experimental datasets like single cell RNA sequencing showing both population delineation by transcriptomics and receptor sequencing [143] will surely unveil new properties of thymic selection, reveal new hidden subpopulations and link cell fate to their TCR sequence.

Recently, a multi-scale dynamical model has been developed covering the earliest steps of intrathymic T-cell development until completion of lineage commitment (i.e. the DN2b stage) [38]. This agent-based model comprises gene regulatory networks, epigenetics and population dynamics based on single-cell gene expression data for key transcription factors as well as in vitro differentiation and proliferation dynamics of populations and individual clones. Experimental data had revealed that expression of the T-lineage commitment Bcl11b is subject to complex regulatory mechanisms involving an interplay of cis-acting and trans-acting elements in combination with a degree of stochasticity [144]. Furthermore, simple gene regulatory networks were not able to fully explain observed and modelled population dynamics of immature thymocytes, which we extensively discussed in Section 2. This type of multi-scale model allows for a smooth transition between differentiation stages, going beyond the 'yes-or-no' gating strategies shown in Figure 1A, and could reveal unexpected cell conversion or differentiation

 doi:10.20944/preprints202101.0388.v1

pathways in the future. Together, this study highlights the requirement of extensive and complementary datasets to build a mathematical model with sufficient explanatory power as well as the requirement for multi-scale approaches to adequately represent the increasing level of detail of our moleculatr, cellular and organismal knowledge of developmental processes.

6. Outlook

We aimed to provide a broad overview of scales of intrathymic T-cell development that have been simulated by mathematical modelling, where the same mechanisms are treated from different angles and data types. Modelling has been necessary to infer hidden experimental information at the cellular (proliferation speed, death) or population scales (developmental dynamics), or to understand fundamental properties of this complex selection system. The next generation of models will most likely include multi-scale datasets, like proliferation speed, population dynamics, as well as signaling, and will likely be single-cell based.

T-cell developmental dynamics as a model system highlights the diversity of modelling methods used at the same scale, and the complexity to measure and bridge cellular events to population dynamics. ODE models are not always best suited, due to their assumption that cells stay with an exponentially distributed time before leaving, and might require special care in their design or interpretation. Generational models can replace logistic growth mechanisms, suggesting that controlled number of divisions is a potential homeostatic mechanism for a fast thymic reconstitution. Dynamical models were powerful at hypothesis testing, by providing the most suited mechanistic scenario to explain the datasets, but were poorly able to identify biological parameters from experimental datasets. Underlying reasons were either parameter uncertainties (only few studies actually showed identifiability of their parameters) or model uncertainties (that another model structure would cause the model to infer different parameter values). Rigorous testing of different possible model structures requires a dissuasive amount of work. As a consequence, no consensus on the proliferation, death (although quite close) or differentiation rates during T-cell development has been reached, despite the large extent of datasets. Given the diversity of datasets and complex experimental setups, these datasets remain difficult to combine. A more general question would be: what is missing from these datasets to finally infer these biological rates? Or which perturbations would be needed to actually identify the strength of competition or regulation between populations? The panel of models reviewed here may provide cues to design next generation multiscale models.

Author Contributions: "Conceptualization, PA.R., H.K-S., V.G., A.K.; methodology, PA.R., H.K-S., V.G., A.K.; software, N.A.; validation, N.A.; formal analysis, N.A.; investigation, PA.R., H.K-S., V.G., A.K.; resources, PA.R., H.K-S., V.G., A.K.; data curation, PA.R., H.K-S., V.G., A.K.; writing—original draft preparation, PA.R., H.K-S., V.G., A.K.; writing—review and editing, PA.R., H.K-S., V.G., A.K.; visualization, PA.R., H.K-S., V.G., A.K.; supervision, PA.R., H.K-S., V.G., A.K.; project administration, N.A.; funding acquisition, PA.R., H.K-S., V.G., A.K. All authors have read and agreed to the published version of the manuscript.

Funding: support was provided by The Helmsley Charitable Trust (#2019PG-T1D011, to VG), UiO World-Leading Research Community (to VG), UiO:LifeSciences Convergence Environment Immunolingo (to VG), EU Horizon 2020 iReceptorplus (#825821) (to VG), a Research Council of Norway FRIPRO project (#300740, to VG). Work on quantitative biology of T-cell development in the laboratory of A.K. is funded by the German Research Foundation (DFG, grant KR2320/6-1).

 doi:10.20944/preprints202101.0388.v1

Conflicts of Interest: The authors declare no conflict of interest. The funders had no role in the design of the study; in the collection, analyses, or interpretation of data; in the writing of the manuscript, or in the decision to publish the results.

Abbreviations

The following abbreviations are used in this manuscript:

APC	Antigen Presenting Cell
BrdU	Bromodeoxyuridine
CLP	Common Lymphoid Progenitor
CD4SP	Single Positive $CD4^+CD8^-$ thymocyte
CD8SP	Single Positive $CD4^-CD8^+$ thymocyte
DC	Dendritic Cell
DN	Double Negative thymocyte
DP	Double Positive thymocyte
EdU	5-Ethynyl-2′-deoxyuridine
ETP	Early T-lineage Progenitor
ISP8	Immature Single Positive $CD8^+$ thymocyte
LMPP	Lymphoid-Primed Multipotent Progenitors
MHC	Major Histocompatibility Complex
ODE	Ordinary Differential Equation
SP	Single Positive thymocyte
TCR	T-cell Receptor
TRA	Tissue Restricted Antigen
Treg	Regulatory T-cell

References

1. Krueger, A. Thymus colonization: who, how, how many? *Archivum Immunologiae et Therapiae Experimentalis* **2018**, *66*, 81–88.
2. Peaudecerf, L.; Lemos, S.; Galgano, A.; Krenn, G.; Vasseur, F.; Di Santo, J.P.; Ezine, S.; Rocha, B. Thymocytes may persist and differentiate without any input from bone marrow progenitors. *Journal of Experimental Medicine* **2012**, *209*, 1401–1408.
3. Martins, V.C.; Ruggiero, E.; Schlenner, S.M.; Madan, V.; Schmidt, M.; Fink, P.J.; von Kalle, C.; Rodewald, H.R. Thymus-autonomous T cell development in the absence of progenitor import. *Journal of Experimental Medicine* **2012**, *209*, 1409–1417.
4. Ansari, A.R.; Liu, H. Acute thymic involution and mechanisms for recovery. *Archivum Immunologiae et Therapiae Experimentalis* **2017**, *65*, 401–420.
5. Godfrey, D.I.; Uldrich, A.P.; McCluskey, J.; Rossjohn, J.; Moody, D.B. The burgeoning family of unconventional T cells. *Nature immunology* **2015**, *16*, 1114.
6. Au-Yeung, B.B.; Melichar, H.J.; Ross, J.O.; Cheng, D.A.; Zikherman, J.; Shokat, K.M.; Robey, E.A.; Weiss, A. Quantitative and temporal requirements revealed for Zap70 catalytic activity during T cell development. *Nature immunology* **2014**, *15*, 687–694.
7. Mariathasan, S.; Zakarian, A.; Bouchard, D.; Michie, A.M.; Zúñiga-Pflücker, J.C.; Ohashi, P.S. Duration and strength of extracellular signal-regulated kinase signals are altered during positive versus negative thymocyte selection. *The Journal of Immunology* **2001**, *167*, 4966–4973.
8. Werlen, G.; Hausmann, B.; Palmer, E. A motif in the $\alpha\beta$ T-cell receptor controls positive selection by modulating ERK activity. *Nature* **2000**, *406*, 422–426.
9. McNeil, L.K.; Starr, T.K.; Hogquist, K.A. A requirement for sustained ERK signaling during thymocyte positive selection in vivo. *Proceedings of the National Academy of Sciences* **2005**, *102*, 13574–13579.
10. Daniels, M.A.; Teixeiro, E.; Gill, J.; Hausmann, B.; Roubaty, D.; Holmberg, K.; Werlen, G.; Holländer, G.A.; Gascoigne, N.R.; Palmer, E. Thymic selection threshold defined by compartmentalization of Ras/MAPK signalling. *Nature* **2006**, *444*, 724–729.
11. Palmer, E.; Naeher, D. Affinity threshold for thymic selection through a T-cell receptor–co-receptor zipper. *Nature Reviews Immunology* **2009**, *9*, 207–213.
12. Yates, A. Theories and quantification of thymic selection. *Frontiers in immunology* **2014**, *5*, 13.
13. Krueger, A.; Ziętara, N.; Łyszkiewicz, M. T cell development by the numbers. *Trends in immunology* **2017**, *38*, 128–139.
14. Wu, L.; Scollay, R.; Egerton, M.; Pearse, M.; Spangrude, G.J.; Shortman, K. CD4 expressed on earliest T-lineage precursor cells in the adult murine thymus. *Nature* **1991**, *349*, 71–74.
15. Allman, D.; Sambandam, A.; Kim, S.; Miller, J.P.; Pagan, A.; Well, D.; Meraz, A.; Bhandoola, A. Thymopoiesis independent of common lymphoid progenitors. *Nature immunology* **2003**, *4*, 168–174.

16. Foss, D.L.; Donskoy, E.; Goldschneider, I. The importation of hematogenous precursors by the thymus is a gated phenomenon in normal adult mice. *The Journal of experimental medicine* **2001**, *193*, 365–374.
17. Ziętara, N.; Łyszkiewicz, M.; Puchałka, J.; Witzlau, K.; Reinhardt, A.; Förster, R.; Pabst, O.; Prinz, I.; Krueger, A. Multicongenic fate mapping quantification of dynamics of thymus colonization. *Journal of Experimental Medicine* **2015**, *212*, 1589–1601.
18. Gossens, K.; Naus, S.; Corbel, S.Y.; Lin, S.; Rossi, F.M.; Kast, J.; Ziltener, H.J. Thymic progenitor homing and lymphocyte homeostasis are linked via S1P-controlled expression of thymic P-selectin/CCL25. *Journal of Experimental Medicine* **2009**, *206*, 761–778.
19. Donskoy, E.; Foss, D.; Goldschneider, I. Gated importation of prothymocytes by adult mouse thymus is coordinated with their periodic mobilization from bone marrow. *The Journal of Immunology* **2003**, *171*, 3568–3575.
20. Godfrey, D.I.; Kennedy, J.; Suda, T.; Zlotnik, A. A developmental pathway involving four phenotypically and functionally distinct subsets of CD3-CD4-CD8-triple-negative adult mouse thymocytes defined by CD44 and CD25 expression. *The Journal of Immunology* **1993**, *150*, 4244–4252.
21. Ceredig, R.; Lowenthal, J.W.; Nabholz, M.; Macdonald, H.R. Expression of interleukin-2 receptors as a differentiation marker on intrathymic stem cells. *Nature* **1985**, *314*, 98–100.
22. Tan, C.; Taylor, A.A.; Coburn, M.Z.; Marino, J.H.; Van De Wiele, C.J.; Teague, T.K. Ten-color flow cytometry reveals distinct patterns of expression of CD124 and CD126 by developing thymocytes. *BMC immunology* **2011**, *12*, 36.
23. Yui, M.A.; Feng, N.; Rothenberg, E.V. Fine-scale staging of T cell lineage commitment in adult mouse thymus. *The Journal of Immunology* **2010**, *185*, 284–293.
24. Porritt, H.E.; Gordon, K.; Petrie, H.T. Kinetics of steady-state differentiation and mapping of intrathymic-signaling environments by stem cell transplantation in nonirradiated mice. *The Journal of experimental medicine* **2003**, *198*, 957–962.
25. Manesso, E.; Chickarmane, V.; Kueh, H.Y.; Rothenberg, E.V.; Peterson, C. Computational modelling of T-cell formation kinetics: output regulated by initial proliferation-linked deferral of developmental competence. *Journal of The Royal Society Interface* **2013**, *10*, 20120774.
26. Zhou, W.; Yui, M.A.; Williams, B.A.; Yun, J.; Wold, B.J.; Cai, L.; Rothenberg, E.V. Single-cell analysis reveals regulatory gene expression dynamics leading to lineage commitment in early T cell development. *Cell systems* **2019**, *9*, 321–337.
27. Schlenner, S.M.; Madan, V.; Busch, K.; Tietz, A.; Läufle, C.; Costa, C.; Blum, C.; Fehling, H.J.; Rodewald, H.R. Fate mapping reveals separate origins of T cells and myeloid lineages in the thymus. *Immunity* **2010**, *32*, 426–436.
28. Saran, N.; Łyszkiewicz, M.; Pommerencke, J.; Witzlau, K.; Vakilzadeh, R.; Ballmaier, M.; von Boehmer, H.; Krueger, A. Multiple extrathymic precursors contribute to T-cell development with different kinetics. *Blood, The Journal of the American Society of Hematology* **2010**, *115*, 1137–1144.
29. Cai, A.Q.; Landman, K.A.; Hughes, B.D.; Witt, C.M. T cell development in the thymus: from periodic seeding to constant output. *Journal of theoretical biology* **2007**, *249*, 384–394.
30. Belyaev, N.N.; Brown, D.E.; Diaz, A.I.G.; Rae, A.; Jarra, W.; Thompson, J.; Langhorne, J.; Potocnik, A.J. Induction of an IL7-R+ c-Kit hi myelolymphoid progenitor critically dependent on IFN-γ signaling during acute malaria. *Nature immunology* **2010**, *11*, 477–485.
31. Chen, E.L.; Thompson, P.K.; Zúñiga-Pflücker, J.C. RBPJ-dependent Notch signaling initiates the T cell program in a subset of thymus-seeding progenitors. *Nature immunology* **2019**, *20*, 1456–1468.
32. Groettrup, M.; Ungewiss, K.; Azogui, O.; Palacios, R.; Owen, M.J.; Hayday, A.C.; von Boehmer, H. A novel disulfide-linked heterodimer on pre—T cells consists of the T cell receptor β chain and a 33 kd glycoprotein. *Cell* **1993**, *75*, 283–294.
33. Pénit, C.; Lucas, B.; Vasseur, F. Cell expansion and growth arrest phases during the transition from precursor (CD4-8-) to immature (CD4+ 8+) thymocytes in normal and genetically modified mice. *The Journal of Immunology* **1995**, *154*, 5103–5113.
34. Stritesky, G.L.; Xing, Y.; Erickson, J.R.; Kalekar, L.A.; Wang, X.; Mueller, D.L.; Jameson, S.C.; Hogquist, K.A. Murine thymic selection quantified using a unique method to capture deleted T cells. *Proceedings of the National Academy of Sciences* **2013**, *110*, 4679–4684.
35. Hare, K.J.; Wilkinson, R.W.; Jenkinson, E.J.; Anderson, G. Identification of a developmentally regulated phase of postselection expansion driven by thymic epithelium. *The Journal of Immunology* **1998**, *160*, 3666–3672.
36. Föhse, L.; Reinhardt, A.; Oberdörfer, L.; Schmitz, S.; Förster, R.; Malissen, B.; Prinz, I. Differential postselection proliferation dynamics of $\alpha\beta$ T cells, Foxp3+ regulatory T cells, and invariant NKT cells monitored by genetic pulse labeling. *The Journal of Immunology* **2013**, *191*, 2384–2392.
37. Le Campion, A.; Lucas, B.; Dautigny, N.; Léaument, S.; Vasseur, F.; Pénit, C. Quantitative and qualitative adjustment of thymic T cell production by clonal expansion of premigrant thymocytes. *The Journal of Immunology* **2002**, *168*, 1664–1671.
38. Olariu, V.; Yui, M.; Krupinski, P.; Zhou, W.; Deichmann, J.; Rothenberg, E.; Peterson, C. Multi-scale dynamical modelling of T-cell development from an early thymic progenitor state to lineage commitment. *Cell Reports* **2020**, *34*, 108622.
39. Egerton, M.; Scollay, R.; Shortman, K. Kinetics of mature T-cell development in the thymus. *Proceedings of the National Academy of Sciences* **1990**, *87*, 2579–2582.
40. Egerton, M.; Shortman, K.; Scollay, R. The kinetics of immature murine thymocyte development in vivo. *International immunology* **1990**, *2*, 501–507.
41. Yap, J.Y.; others. Quantitative dissection of T cell negative selection mechanisms in the thymus **2017**.

42. McCaughtry, T.M.; Wilken, M.S.; Hogquist, K.A. Thymic emigration revisited. *Journal of Experimental Medicine* **2007**, *204*, 2513–2520.
43. Sinclair, C.; Seddon, B. Overlapping and asymmetric functions of TCR signaling during thymic selection of CD4 and CD8 lineages. *The Journal of Immunology* **2014**, *192*, 5151–5159.
44. Sinclair, C.; Bains, I.; Yates, A.J.; Seddon, B. Asymmetric thymocyte death underlies the CD4: CD8 T-cell ratio in the adaptive immune system. *Proceedings of the National Academy of Sciences* **2013**, *110*, E2905–E2914.
45. Mehr, R.; Globerson, A.; Perelson, A.S. Modeling positive and negative selection and differentiation processes in the thymus. *Journal of theoretical biology* **1995**, *175*, 103–126.
46. Sawicka, M.; Stritesky, G.; Reynolds, J.; Abourashchi, N.; Lythe, G.; Molina-París, C.; Hogquist, K. From pre-DP, post-DP, SP4, and SP8 thymocyte cell counts to a dynamical model of cortical and medullary selection. *Frontiers in immunology* **2014**, *5*, 19.
47. Chiba, K. FTY720, a new class of immunomodulator, inhibits lymphocyte egress from secondary lymphoid tissues and thymus by agonistic activity at sphingosine 1-phosphate receptors. *Pharmacology & therapeutics* **2005**, *108*, 308–319.
48. Wei, T.; Zhang, N.; Guo, Z.; Chi, F.; Song, Y.; Zhu, X. Wnt4 signaling is associated with the decrease of proliferation and increase of apoptosis during age-related thymic involution. *Molecular medicine reports* **2015**, *12*, 7568–7576.
49. Carbajosa, S.; Gea, S.; Chillón-arinas, C.; Poveda, C.; del Carmen Maza, M.; Fresno, M.; Gironès, N. Altered bone marrow lymphopoiesis and interleukin-6-dependent inhibition of thymocyte differentiation contribute to thymic atrophy during Trypanosoma cruzi infection. *Oncotarget* **2017**, *8*, 17551.
50. Zoller, A.L.; Kersh, G.J. Estrogen induces thymic atrophy by eliminating early thymic progenitors and inhibiting proliferation of β-selected thymocytes. *The Journal of Immunology* **2006**, *176*, 7371–7378.
51. Zoller, A.L.; Schnell, F.J.; Kersh, G.J. Murine pregnancy leads to reduced proliferation of maternal thymocytes and decreased thymic emigration. *Immunology* **2007**, *121*, 207–215.
52. Nunes-Alves, C.; Nobrega, C.; Behar, S.M.; Correia-Neves, M. Tolerance has its limits: how the thymus copes with infection. *Trends in immunology* **2013**, *34*, 502–510.
53. Vogel, A.B.; Haasbach, E.; Reiling, S.J.; Droebner, K.; Klingel, K.; Planz, O. Highly pathogenic influenza virus infection of the thymus interferes with T lymphocyte development. *The Journal of Immunology* **2010**, *185*, 4824–4834.
54. Thomas-Vaslin, V.; Altes, H.K.; de Boer, R.J.; Klatzmann, D. Comprehensive assessment and mathematical modeling of T cell population dynamics and homeostasis. *The Journal of Immunology* **2008**, *180*, 2240–2250.
55. Elfaki, Y.; Robert, P.A.; Binz, C.; Falk, C.S.; Bruder, D.; Prinz, I.; Floess, S.; Meyer-Hermann, M.; Huehn, J. Influenza A virus-induced thymus atrophy differentially affects dynamics of conventional and regulatory T cell development. *bioRxiv* **2020**.
56. Moleriu, R.D.; Zaharie, D.; Moatar-Moleriu, L.C.; Gruia, A.T.; Mic, A.A.; Mic, F.A. Insights into the mechanisms of thymus involution and regeneration by modeling the glucocorticoid-induced perturbation of thymocyte populations dynamics. *Journal of Theoretical Biology* **2014**, *348*, 80–99.
57. Hu, D.Y.; Yap, J.Y.; Wirasinha, R.C.; Howard, D.R.; Goodnow, C.C.; Daley, S.R. A timeline demarcating two waves of clonal deletion and Foxp3 upregulation during thymocyte development. *Immunology and cell biology* **2016**, *94*, 357–366.
58. Marshall, D.; Sinclair, C.; Tung, S.; Seddon, B. Differential requirement for IL-2 and IL-15 during bifurcated development of thymic regulatory T cells. *The Journal of Immunology* **2014**, *193*, 5525–5533.
59. Cowan, J.E.; Parnell, S.M.; Nakamura, K.; Caamano, J.H.; Lane, P.J.; Jenkinson, E.J.; Jenkinson, W.E.; Anderson, G. The thymic medulla is required for Foxp3+ regulatory but not conventional CD4+ thymocyte development. *Journal of Experimental Medicine* **2013**, *210*, 675–681.
60. Liston, A.; Nutsch, K.M.; Farr, A.G.; Lund, J.M.; Rasmussen, J.P.; Koni, P.A.; Rudensky, A.Y. Differentiation of regulatory Foxp3+ T cells in the thymic cortex. *Proceedings of the National Academy of Sciences* **2008**, *105*, 11903–11908.
61. Łyszkiewicz, M.; Winter, S.J.; Witzlau, K.; Föhse, L.; Brownlie, R.; Puchałka, J.; Verheyden, N.A.; Kunze-Schumacher, H.; Imelmann, E.; Blume, J.; others. miR-181a/b-1 controls thymic selection of Treg cells and tunes their suppressive capacity. *PLoS biology* **2019**, *17*, e2006716.
62. Owen, D.L.; Mahmud, S.A.; Sjaastad, L.E.; Williams, J.B.; Spanier, J.A.; Simeonov, D.R.; Ruscher, R.; Huang, W.; Proekt, I.; Miller, C.N.; others. Thymic regulatory T cells arise via two distinct developmental programs. *Nature immunology* **2019**, *20*, 195–205.
63. Zaharie, D.; Moleriu, R.D.; Mic, F.A. Modeling the development of the post-natal mouse thymus in the absence of bone marrow progenitors. *Scientific reports* **2016**, *6*, 36159.
64. Peschon, J.J.; Morrissey, P.J.; Grabstein, K.H.; Ramsdell, F.J.; Maraskovsky, E.; Gliniak, B.C.; Park, L.S.; Ziegler, S.F.; Williams, D.E.; Ware, C.B.; others. Early lymphocyte expansion is severely impaired in interleukin 7 receptor-deficient mice. *The Journal of experimental medicine* **1994**, *180*, 1955–1960.
65. von Freeden-Jeffry, U.; Vieira, P.; Lucian, L.A.; McNeil, T.; Burdach, S.; Murray, R. Lymphopenia in interleukin (IL)-7 gene-deleted mice identifies IL-7 as a nonredundant cytokine. *Journal of Experimental Medicine* **1995**, *181*, 1519–1526.
66. Almeida, A.R.; Borghans, J.A.; Freitas, A.A. T Cell HomeostasisThymus Regeneration and Peripheral T Cell Restoration in Mice with a Reduced Fraction of Competent Precursors. *Journal of Experimental Medicine* **2001**, *194*, 591–600.
67. Zlotoff, D.A.; Sambandam, A.; Logan, T.D.; Bell, J.J.; Schwarz, B.A.; Bhandoola, A. CCR7 and CCR9 together recruit hematopoietic progenitors to the adult thymus. *Blood, The Journal of the American Society of Hematology* **2010**, *115*, 1897–1905.

68. Krueger, A.; Willenzon, S.; Łyszkiewicz, M.; Kremmer, E.; Förster, R. CC chemokine receptor 7 and 9 double-deficient hematopoietic progenitors are severely impaired in seeding the adult thymus. *Blood, The Journal of the American Society of Hematology* **2010**, *115*, 1906–1912.
69. Ramos, C.V.; Ballesteros-Arias, L.; Silva, J.G.; Paiva, R.A.; Nogueira, M.F.; Carneiro, J.; Gjini, E.; Martins, V.C. Cell Competition, the Kinetics of Thymopoiesis, and Thymus Cellularity Are Regulated by Double-Negative 2 to 3 Early Thymocytes. *Cell Reports* **2020**, *32*, 107910.
70. Apert, C.; Romagnoli, P.; van Meerwijk, J.P. IL-2 and IL-15 dependent thymic development of Foxp3-expressing regulatory T lymphocytes. *Protein & cell* **2018**, *9*, 322–332.
71. Thiault, N.; Darrigues, J.; Adoue, V.; Gros, M.; Binet, B.; Perals, C.; Leobon, B.; Fazilleau, N.; Joffre, O.P.; Robey, E.A.; others. Peripheral regulatory T lymphocytes recirculating to the thymus suppress the development of their precursors. *Nature immunology* **2015**, *16*, 628–634.
72. Klein, L.; Robey, E.A.; Hsieh, C.S. Central CD4+ T cell tolerance: deletion versus regulatory T cell differentiation. *Nature Reviews Immunology* **2019**, *19*, 7–18.
73. Kaneko, K.B.; Tateishi, R.; Miyao, T.; Takakura, Y.; Akiyama, N.; Yokota, R.; Akiyama, T.; Kobayashi, T.J. Quantitative analysis reveals reciprocal regulations underlying recovery dynamics of thymocytes and thymic environment in mice. *Communications biology* **2019**, *2*, 1–11.
74. Binder, S.C.; Hernandez-Vargas, E.A.; Meyer-Hermann, M. Reducing complexity: An iterative strategy for parameter determination in biological networks. *Computer Physics Communications* **2015**, *190*, 15–22.
75. Bandara, S.; Schlöder, J.P.; Eils, R.; Bock, H.G.; Meyer, T. Optimal experimental design for parameter estimation of a cell signaling model. *PLoS Comput Biol* **2009**, *5*, e1000558.
76. Graziano, M.; St-Pierre, Y.; Beauchemin, C.; Desrosiers, M.; Potworowski, E.F. The Fate of Thymocytes Labeledin Vivowith CFSE. *Experimental cell research* **1998**, *240*, 75–85.
77. Kreslavsky, T.; Gleimer, M.; Miyazaki, M.; Choi, Y.; Gagnon, E.; Murre, C.; Sicinski, P.; von Boehmer, H. β-Selection-induced proliferation is required for $\alpha\beta$ T cell differentiation. *Immunity* **2012**, *37*, 840–853.
78. Kuwata, N.; Igarashi, H.; Ohmura, T.; Aizawa, S.; Sakaguchi, N. Cutting edge: absence of expression of RAG1 in peritoneal B-1 cells detected by knocking into RAG1 locus with green fluorescent protein gene. *The Journal of Immunology* **1999**, *163*, 6355–6359.
79. Winter, S.J.; Krueger, A. Development of unconventional T cells controlled by MicroRNA. *Frontiers in immunology* **2019**, *10*, 2520.
80. Bernitz, J.M.; Kim, H.S.; MacArthur, B.; Sieburg, H.; Moore, K. Hematopoietic stem cells count and remember self-renewal divisions. *Cell* **2016**, *167*, 1296–1309.
81. Morcos, M.N.; Zerjatke, T.; Glauche, I.; Munz, C.M.; Ge, Y.; Petzold, A.; Reinhardt, S.; Dahl, A.; Anstee, N.; Bogeska, R.; others. Proliferative behavior of hematopoietic stem cells revisited: No evidence for mitotic memory. *bioRxiv* **2019**, p. 745729.
82. Prinz, I.; Sansoni, A.; Kissenpfennig, A.; Ardouin, L.; Malissen, M.; Malissen, B. Visualization of the earliest steps of $\gamma\delta$ T cell development in the adult thymus. *Nature immunology* **2006**, *7*, 995–1003.
83. Quackenbush, R.; Shields, A. Local re-utilization of thymidine in normal mouse tissues as measured with iododeoxyuridine. *Cell Proliferation* **1988**, *21*, 381–387.
84. Hagan, M. C. Cell Proliferation Kinetics Analyzed with BrdU and Near-UV Light Treatment1. In *Current Methodology in Experimental Hematology*; Karger Publishers, 1984; Vol. 48, pp. 384–401.
85. Matiašová, A.; Ševc, J.; Mikeš, J.; Jendželovskỳ, R.; Daxnerová, Z.; Fedoročko, P. Flow cytometric determination of 5-bromo-2-deoxyuridine pharmacokinetics in blood serum after intraperitoneal administration to rats and mice. *Histochemistry and cell biology* **2014**, *142*, 703–712.
86. Vogel, K.U.; Bell, L.S.; Galloway, A.; Ahlfors, H.; Turner, M. The RNA-binding proteins Zfp36l1 and Zfp36l2 enforce the thymic β-selection checkpoint by limiting DNA damage response signaling and cell cycle progression. *The Journal of Immunology* **2016**, *197*, 2673–2685.
87. Bonhoeffer, S.; Mohri, H.; Ho, D.; Perelson, A.S. Quantification of cell turnover kinetics using 5-bromo-2-deoxyuridine1. *The Journal of Immunology* **2000**, *164*, 5049–5054.
88. Baron, C.; Pénit, C. Study of the thymocyte cell cycle by bivariate analysis of incorporated bromodeoxyuridine and DNA content. *European journal of immunology* **1990**, *20*, 1231–1236.
89. Vibert, J.; Thomas-Vaslin, V. Modelling T cell proliferation: Dynamics heterogeneity depending on cell differentiation, age, and genetic background. *PLoS computational biology* **2017**, *13*, e1005417.
90. Ramos, C.V.; Ballesteros-Arias, L.; Silva, J.G.; Nogueira, M.; Gjini, E.; Martins, V.C. Cell competition regulates the kinetics of thymopoiesis and thymus cellularity. *bioRxiv* **2019**.
91. Jolly, A.; Fanti, A.K.; Gräßer, I.; Becker, N.B.; Höfer, T. CycleFlow quantifies cell-cycle heterogeneity in vivo. *bioRxiv* **2020**.
92. Gitlin, A.D.; Mayer, C.T.; Oliveira, T.Y.; Shulman, Z.; Jones, M.J.; Koren, A.; Nussenzweig, M.C. T cell help controls the speed of the cell cycle in germinal center B cells. *Science* **2015**, *349*, 643–646.
93. Kretschmer, L.; Flossdorf, M.; Mir, J.; Cho, Y.L.; Plambeck, M.; Treise, I.; Toska, A.; Heinzel, S.; Schiemann, M.; Busch, D.H.; others. Differential expansion of T central memory precursor and effector subsets is regulated by division speed. *Nature communications* **2020**, *11*, 1–12.
94. Weber, T.S.; Jaehnert, I.; Schichor, C.; Or-Guil, M.; Carneiro, J. Quantifying the length and variance of the eukaryotic cell cycle phases by a stochastic model and dual nucleoside pulse labelling. *PLoS Comput Biol* **2014**, *10*, e1003616.

95. Zilman, A.; Ganusov, V.V.; Perelson, A.S. Stochastic models of lymphocyte proliferation and death. *PLoS one* **2010**, *5*, e12775.
96. Trucco, E. Mathematical models for cellular systems. The von Foerster equation. Part II. *The bulletin of mathematical biophysics* **1965**, *27*, 449–471.
97. Miles, J. The Laplace transform of the lognormal distribution. *arXiv preprint arXiv:1803.05878* **2018**.
98. Bernard, D.; Mondesert, O.; Gomes, A.; Duthen, Y.; Lobjois, V.; Cussat-Blanc, S.; Ducommun, B. A checkpoint-oriented cell cycle simulation model. *Cell Cycle* **2019**, *18*, 795–808.
99. Wellard, C.; Markham, J.F.; Hawkins, E.D.; Hodgkin, P.D. The cyton model for lymphocyte proliferation and differentiation. In *Mathematical Models and Immune Cell Biology*; Springer, 2011; pp. 107–120.
100. Dowling, M.R.; Kan, A.; Heinzel, S.; Zhou, J.H.; Marchingo, J.M.; Wellard, C.J.; Markham, J.F.; Hodgkin, P.D. Stretched cell cycle model for proliferating lymphocytes. *Proceedings of the National Academy of Sciences* **2014**, *111*, 6377–6382.
101. Miller, I.; Min, M.; Yang, C.; Tian, C.; Gookin, S.; Carter, D.; Spencer, S.L. Ki67 is a graded rather than a binary marker of proliferation versus quiescence. *Cell reports* **2018**, *24*, 1105–1112.
102. Zambon, A.C. Use of the Ki67 promoter to label cell cycle entry in living cells. *Cytometry Part A* **2010**, *77*, 564–570.
103. Bains, I.; Thiébaut, R.; Yates, A.J.; Callard, R. Quantifying thymic export: combining models of naive T cell proliferation and TCR excision circle dynamics gives an explicit measure of thymic output. *The Journal of Immunology* **2009**, *183*, 4329–4336.
104. Lahoz-Beneytez, J.; Schaller, S.; Macallan, D.; Eissing, T.; Niederalt, C.; Asquith, B. Physiologically based simulations of deuterated glucose for quantifying cell turnover in humans. *Frontiers in immunology* **2017**, *8*, 474.
105. Sakaue-Sawano, A.; Yo, M.; Komatsu, N.; Hiratsuka, T.; Kogure, T.; Hoshida, T.; Goshima, N.; Matsuda, M.; Miyoshi, H.; Miyawaki, A. Genetically encoded tools for optical dissection of the mammalian cell cycle. *Molecular cell* **2017**, *68*, 626–640.
106. Kurd, N.S.; Lutes, L.K.; Yoon, J.; Chan, S.W.; Dzhagalov, I.L.; Hoover, A.R.; Robey, E.A. A role for phagocytosis in inducing cell death during thymocyte negative selection. *ELife* **2019**, *8*, e48097.
107. Surh, C.D.; Sprent, J. T-cell apoptosis detected in situ during positive and negative selection in the thymus. *Nature* **1994**, *372*, 100–103.
108. Laufer, T.M.; DeKoning, J.; Markowitz, J.S.; Lo, D.; Glimcher, L.H. Unopposed positive selection and autoreactivity in mice expressing class II MHC only on thymic cortex. *Nature* **1996**, *383*, 81–85.
109. van Meerwijk, J.P.; Marguerat, S.; Lees, R.K.; Germain, R.N.; Fowlkes, B.; MacDonald, H.R. Quantitative impact of thymic clonal deletion on the T cell repertoire. *The Journal of experimental medicine* **1997**, *185*, 377–384.
110. Anderson, G.; Partington, K.M.; Jenkinson, E.J. Differential effects of peptide diversity and stromal cell type in positive and negative selection in the thymus. *The Journal of Immunology* **1998**, *161*, 6599–6603.
111. Merkenschlager, M.; Graf, D.; Lovatt, M.; Bommhardt, U.; Zamoyska, R.; Fisher, A.G. How many thymocytes audition for selection? *The Journal of experimental medicine* **1997**, *186*, 1149–1158.
112. Itano, A.; Robey, E. Highly efficient selection of CD4 and CD8 lineage thymocytes supports an instructive model of lineage commitment. *Immunity* **2000**, *12*, 383–389.
113. Daley, S.R.; Hu, D.Y.; Goodnow, C.C. Helios marks strongly autoreactive CD4+ T cells in two major waves of thymic deletion distinguished by induction of PD-1 or NF-κB. *Journal of Experimental Medicine* **2013**, *210*, 269–285.
114. Hogquist, K.A.; Jameson, S.C. The self-obsession of T cells: how TCR signaling thresholds affect fate'decisions' and effector function. *Nature immunology* **2014**, *15*, 815.
115. Grossman, Z.; Singer, A. Tuning of activation thresholds explains flexibility in the selection and development of T cells in the thymus. *Proceedings of the National Academy of Sciences* **1996**, *93*, 14747–14752.
116. Kurd, N.; Robey, E.A. T-cell selection in the thymus: a spatial and temporal perspective. *Immunological reviews* **2016**, *271*, 114–126.
117. Melichar, H.J.; Ross, J.O.; Herzmark, P.; Hogquist, K.A.; Robey, E.A. Distinct temporal patterns of T cell receptor signaling during positive versus negative selection in situ. *Science signaling* **2013**, *6*, ra92–ra92.
118. Melichar, H.J.; Ross, J.O.; Taylor, K.T.; Robey, E.A. Stable interactions and sustained TCR signaling characterize thymocyte–thymocyte interactions that support negative selection. *The Journal of Immunology* **2015**, *194*, 1057–1061.
119. Ross, J.O.; Melichar, H.J.; Halkias, J.; Robey, E.A. Studying T cell development in thymic slices. In *T-Cell Development*; Springer, 2016; pp. 131–140.
120. Khailaie, S.; Robert, P.A.; Toker, A.; Huehn, J.; Meyer-Hermann, M. A signal integration model of thymic selection and natural regulatory T cell commitment. *The Journal of Immunology* **2014**, *193*, 5983–5996.
121. Sant'Angelo, D.B.; Waterbury, P.G.; Cohen, B.E.; Martin, W.D.; Van Kaer, L.; Hayday, A.C.; Janeway Jr, C.A. The imprint of intrathymic self-peptides on the mature T cell receptor repertoire. *Immunity* **1997**, *7*, 517–524.
122. Ebert, P.J.; Jiang, S.; Xie, J.; Li, Q.J.; Davis, M.M. An endogenous positively selecting peptide enhances mature T cell responses and becomes an autoantigen in the absence of microRNA miR-181a. *Nature immunology* **2009**, *10*, 1162.
123. Lo, W.L.; Felix, N.J.; Walters, J.J.; Rohrs, H.; Gross, M.L.; Allen, P.M. An endogenous peptide positively selects and augments the activation and survival of peripheral CD4+ T cells. *Nature immunology* **2009**, *10*, 1155.
124. Vrisekoop, N.; Monteiro, J.P.; Mandl, J.N.; Germain, R.N. Revisiting thymic positive selection and the mature T cell repertoire for antigen. *Immunity* **2014**, *41*, 181–190.
125. Burroughs, N.J.; de Boer, R.J.; Keşmir, C. Discriminating self from nonself with short peptides from large proteomes. *Immunogenetics* **2004**, *56*, 311–320.

126. Ganti, R.S.; Lo, W.L.; McAffee, D.B.; Groves, J.T.; Weiss, A.; Chakraborty, A.K. How the T cell signaling network processes information to discriminate between self and agonist ligands. *Proceedings of the National Academy of Sciences* **2020**, *117*, 26020–26030.
127. Nitta, T.; Tsutsumi, M.; Nitta, S.; Muro, R.; Suzuki, E.C.; Nakano, K.; Tomofuji, Y.; Sawa, S.; Okamura, T.; Penninger, J.M.; others. Fibroblasts as a source of self-antigens for central immune tolerance. *Nature Immunology* **2020**, *21*, 1172–1180.
128. Brown, C.C.; Rudensky, A.Y. Conceiving the inconceivable: the function of Aire in immune tolerance to peripheral tissue-restricted antigens in the thymus. *The Journal of Immunology* **2021**, *206*, 245–247.
129. Breed, E.R.; Lee, S.T.; Hogquist, K.A. Directing T cell fate: How thymic antigen presenting cells coordinate thymocyte selection. Seminars in cell & developmental biology. Elsevier, 2018, Vol. 84, pp. 2–10.
130. Cosway, E.J.; Ohigashi, I.; Schauble, K.; Parnell, S.M.; Jenkinson, W.E.; Luther, S.; Takahama, Y.; Anderson, G. Formation of the intrathymic dendritic cell pool requires CCL21-mediated recruitment of CCR7+ progenitors to the thymus. *The Journal of Immunology* **2018**, *201*, 516–523.
131. Hu, Z.; Li, Y.; Van Nieuwenhuijze, A.; Selden, H.J.; Jarrett, A.M.; Sorace, A.G.; Yankeelov, T.E.; Liston, A.; Ehrlich, L.I. CCR7 modulates the generation of thymic regulatory T cells by altering the composition of the thymic dendritic cell compartment. *Cell reports* **2017**, *21*, 168–180.
132. Davalos-Misslitz, A.C.; Worbs, T.; Willenzon, S.; Bernhardt, G.; Förster, R. Impaired responsiveness to T-cell receptor stimulation and defective negative selection of thymocytes in CCR7-deficient mice. *Blood, The Journal of the American Society of Hematology* **2007**, *110*, 4351–4359.
133. Garg, G.; Nikolouli, E.; Hardtke-Wolenski, M.; Toker, A.; Ohkura, N.; Beckstette, M.; Miyao, T.; Geffers, R.; Floess, S.; Gerdes, N.; others. Unique properties of thymic antigen-presenting cells promote epigenetic imprinting of alloantigen-specific regulatory T cells. *Oncotarget* **2017**, *8*, 35542.
134. Efroni, S.; Harel, D.; Cohen, I.R. Toward rigorous comprehension of biological complexity: modeling, execution, and visualization of thymic T-cell maturation. *Genome research* **2003**, *13*, 2485–2497.
135. Starruß, J.; de Back, W.; Brusch, L.; Deutsch, A. Morpheus: a user-friendly modeling environment for multiscale and multicellular systems biology. *Bioinformatics* **2014**, *30*, 1331–1332.
136. Efroni, S.; Harel, D.; Cohen, I.R. Emergent dynamics of thymocyte development and lineage determination. *PLoS Comput Biol* **2007**, *3*, e13.
137. Souza-e Silva, H.; Savino, W.; Feijóo, R.A.; Vasconcelos, A.T.R. A cellular automata-based mathematical model for thymocyte development. *PloS one* **2009**, *4*, e8233.
138. Textor, J.; Henrickson, S.E.; Mandl, J.N.; Von Andrian, U.H.; Westermann, J.; De Boer, R.J.; Beltman, J.B. Random migration and signal integration promote rapid and robust T cell recruitment. *PLoS Comput Biol* **2014**, *10*, e1003752.
139. Rastogi, A.; Robert, P.A.; Halle, S.; Meyer-Hermann, M. Evaluation of CD8 T cell killing models with computer simulations of 2-photon imaging experiments. *PLOS Computational Biology* **2020**, *16*, e1008428.
140. Brown, A.J.; Snapkov, I.; Akbar, R.; Pavlović, M.; Miho, E.; Sandve, G.K.; Greiff, V. Augmenting adaptive immunity: progress and challenges in the quantitative engineering and analysis of adaptive immune receptor repertoires. *Molecular Systems Design & Engineering* **2019**, *4*, 701–736.
141. Marcou, Q.; Mora, T.; Walczak, A.M. High-throughput immune repertoire analysis with IGoR. *Nature communications* **2018**, *9*, 1–10.
142. Pei, W.; Feyerabend, T.B.; Rössler, J.; Wang, X.; Postrach, D.; Busch, K.; Rode, I.; Klapproth, K.; Dietlein, N.; Quedenau, C.; others. Polylox barcoding reveals haematopoietic stem cell fates realized in vivo. *Nature* **2017**, *548*, 456–460.
143. Park, J.E.; Botting, R.A.; Conde, C.D.; Popescu, D.M.; Lavaert, M.; Kunz, D.J.; Goh, I.; Stephenson, E.; Ragazzini, R.; Tuck, E.; others. A cell atlas of human thymic development defines T cell repertoire formation. *Science* **2020**, *367*.
144. Hosokawa, H.; Rothenberg, E.V. How transcription factors drive choice of the T cell fate. *Nature Reviews Immunology* **2020**, pp. 1–15.